THE ANATOMICAL RECORD PART A 286A:781–803 (2005)

Cement Lines of Secondary Osteons in Human Bone Are Not Mineral-Deficient: New Data in a Historical Perspective

JOHN G. SKEDROS,[1]* JENNIFER L. HOLMES,[1] ERIC G. VAJDA,[1,2] AND ROY D. BLOEBAUM[1]

[1]Bone and Joint Research Laboratory, Department of Veterans Affairs Medical Center, Salt Lake City, Utah

[2]Ligand Pharmaceuticals, Inc., San Diego, California

ABSTRACT

Using qualitative backscattered electron (BSE) imaging and quantitative energy dispersive X-ray (EDX) spectroscopy, some investigators have concluded that cement (reversal) lines located at the periphery of secondary osteons are poorly mineralized viscous interfaces with respect to surrounding bone. This conclusion contradicts historical observations of apparent highly mineralized (or collagen-deficient) cement lines in microradiographs. Such conclusions, however, may stem from unrecognized artifacts that can occur during scanning electron microscopy. These include specimen degradation due to high-energy beams and the sampling of electron interaction volumes that extend beyond target locations during EDX analysis. This study used quantitative BSE imaging and EDX analysis, each with relatively lower-energy beams, to test the hypothesis that cement lines are poorly mineralized. Undemineralized adult human femoral diaphyses (n = 8) and radial diaphyses (n = 5) were sectioned transversely, embedded in polymethyl methacrylate, and imaged in a scanning electron microscope for BSE and EDX analyses. Unembedded samples were also evaluated. Additional thin embedded samples were stained and evaluated with light microscopy and correlated BSE imaging. BSE analyses showed the consistent presence of a bright line (higher atomic number) coincident with the classical location and description of the cement line. This may represent relative hypermineralization or, alternatively, collagen deficiency with respect to surrounding bone. EDX analyses of cement lines showed either higher Ca content or equivalent Ca content when compared to distant osteonal and interstitial bone. These data reject the hypothesis that cement lines of secondary osteons are poorly mineralized.

Key words: cement line; reversal line; osteons; backscattered electron imaging; cortical bone; bone microdamage

Grant sponsor: the Office of Research and Development Medical Research Service, Department of Veterans Affairs Salt Lake City Health Care System; Grant sponsor: Department of Orthopedics, University of Utah School of Medicine; Grant sponsor: the Utah Bone and Joint Center.

*Correspondence to: John G. Skedros, Utah Bone and Joint Center, 5323 South Woodrow Street, Suite 202, Salt Lake City, UT 84107. Fax: 801-713-0609.
E-mail: jskedros@utahboneandjoint.com

Received 6 November 2003; Accepted 13 December 2004
DOI 10.1002/ar.a.20214
Published online 21 July 2005 in Wiley InterScience (www.interscience.wiley.com).

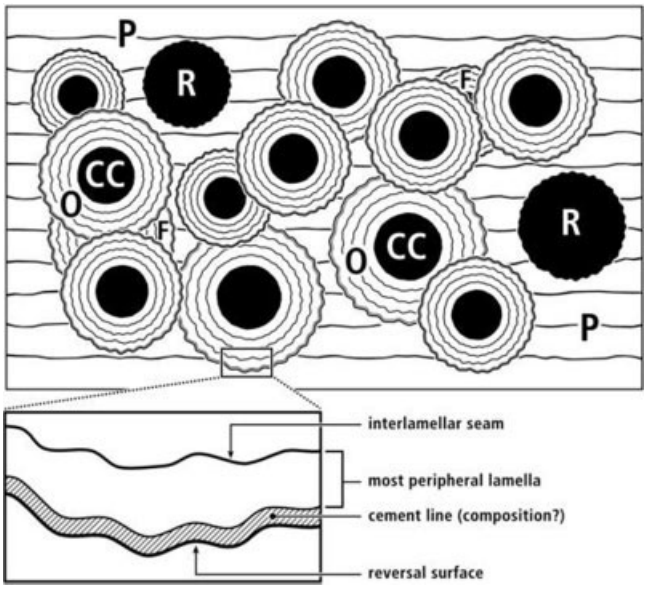

Fig. 1. Diagrammatic representation of human cortical bone from a long bone diaphysis showing secondary osteons (O; Haversian systems) and their central canals (CC), secondary osteon fragments (F), and resorption spaces (R). Two of each characteristic are labeled. Primary bone (P) is indicated by parallel lines. Primary osteons and primary vascular canals are not shown. The outer margin of the resorption space represents the reversal surface. The material formed on this surface, which is peripheral to the outermost osteon lamella, is the cement line (see enlarged portion at bottom). The composition of this region is not completely known.

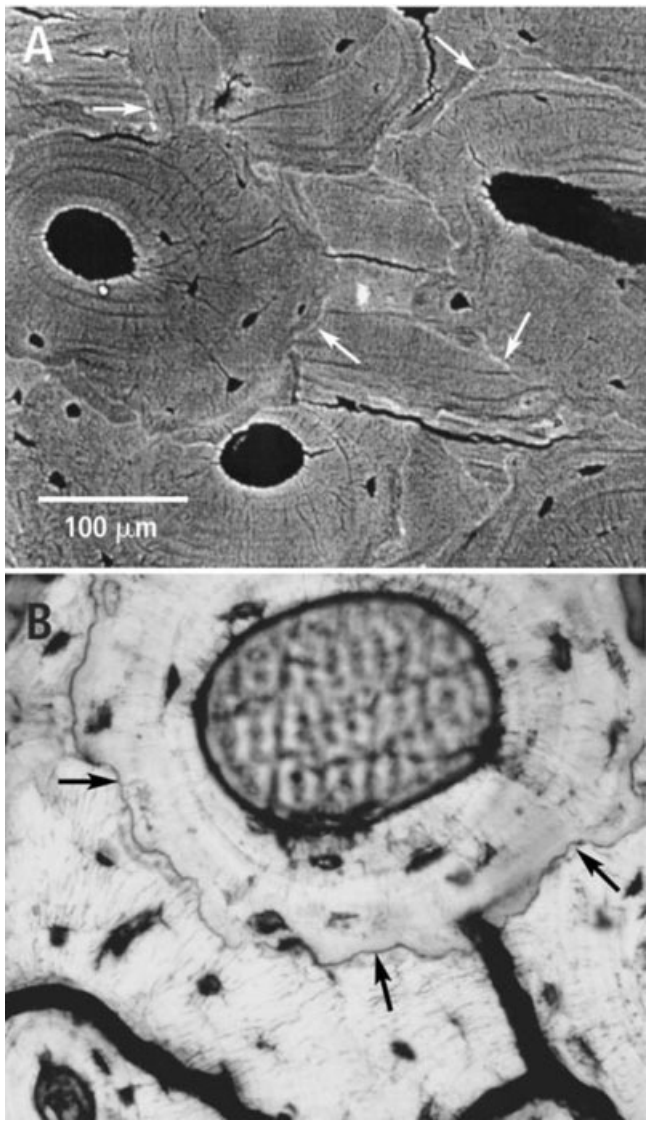

Fig. 2. **A:** Backscattered electron image of adult human femoral cortical bone (undemineralized and PMMA-embedded; transverse section, anterior cortex, mid-diaphysis). Contrary to the hypothesis tested in this study, these images show thin bright lines (presumably highly mineralized) along the peripheral margins of the secondary osteons (arrows). **B:** Transmitted light image of a secondary osteon in adult human femoral cortical bone (undemineralized and PMMA-embedded; transverse section, anterior cortex, mid-diaphysis) that has been stained with basic fuchsin and methylene blue in a buffered acetate solution. Stain uptake is greatest along a scalloped (crenulated) line at the osteon periphery (arrows). This line surrounds the entire osteon and is considered the cement line. The large black features at the bottom of the image are cracks in the bone, an artifact of specimen preparation. These images demonstrate the topographic correspondence of bright lines seen in the backscattered electron images (A) with traditionally appearing cement lines seen in the light microscope (B).

Remodeling of bone involves two major steps: resorption of bone by osteoclasts and formation of new bone by osteoblasts (Frost, 1990; Parfitt, 1994). During remodeling, osteoclasts create a resorption space. The reversal surface that remains represents the physical demarcation where bone resorption reverses to bone formation (Sokolof, 1973; Parfitt, 1984; de Ricqlès et al., 1991; Zhou et al., 1994). The initial material(s) deposited on this reversal surface appears as a thin line in transverse sections or a sheath in three-dimensional space. This thin layer, which may not be homogeneous, represents the reversal or cement line (Figs. 1 and 2). In diaphyseal cortical bone, cement lines typically appear as narrow seams less than 5 μm wide that often exhibit subtle undulations (crenulated or scalloped appearance, corresponding to osteoclast Howship's lacunae) at the periphery of secondary osteons (Sissons, 1962; Ham and Cormack, 1979: p. 441–442; Castanet, 1981; Martin and Burr, 1989: p. 49–51). According to some investigators, cement lines are absent in primary bone because they are by definition associated with the resorption of primary or secondary bone and the formation of secondary bone (Pritchard, 1972; Sokolof, 1973; Jee, 1983; Currey, 1984: p. 29, 47; de Ricqlès et al., 1991; Fawcett, 1994: p. 224; Zhou et al., 1994) (see Appendix).

Von Ebner (1875) first described the cement line as "kittlinien" (putty line or glue line). More recent investigators have published microradiographs showing that cement lines often have brighter gray levels (indicative of higher mineral content) than surrounding bone (Amprino and Engström, 1952; Jowsey, 1960, 1964, 1966; Smith, 1963; Philipson, 1965; Heuck, 1971; Lacroix, 1971; Yaeger, 1971; Dhem and Robert, 1986). Consequently, the cement line has been described as a relatively highly mineralized material, implying a relatively brittle interface (Philipson, 1965; Castanet, 1981; Currey, 1984: p. 46;

Parfitt, 1984). However, the relative mineralization of the cement line with respect to adjacent bone remains controversial. The composition and mineralization of cement lines of secondary osteons (Haversian systems) and their potential influences on bone biomechanical and metabolic functions have been considered many times since their original description by Von Ebner (1875), yet these issues remain unresolved (Schmidt, 1959; Sokolof, 1973; Castanet, 1981; Currey, 1984: p. 47; Schaffler et al., 1987; Burr et al., 1988; Martin and Burr, 1989: p. 51–52; de Ricqlès et al., 1991; Zhou et al., 1994; Zioupos and Currey, 1994; McKee and Nanci, 1995; Brunski et al., 2000; Everts et al., 2002).

Detailed knowledge of the structure and composition of cement lines and adjacent bone is relevant in both clinical and biomechanical contexts. In some bone diseases, such as Paget's disease, cement lines are prolific and have an abnormal appearance and possibly abnormal composition and function (Heuck, 1971, 1993; Rosenberg, 1994), whereas in other diseases, such as rickets (Jowsey, 1966; Boyde et al., 1986), cement lines are absent, suggesting changes in mineralization rates and quality of bone tissue deposited. Cement lines may also influence fatigue properties of bone by attenuating or arresting the propagation of microcracks that form in normal bone (Currey, 1984: p. 264–265, 2002: p. 91; Burr et al., 1985, 1988; Advani et al., 1987; Martin and Burr, 1989: p. 198–201; Choi and Goldstein, 1992; Norman et al., 1995; Schaffler et al., 1995; Prendergast and Huiskes, 1996; Braidotti et al., 1997; Norman and Wang, 1997; Boyce et al., 1998; Guo et al., 1998; Yeni and Norman, 2000; O'Brien et al., 2003; Sobelman et al., 2004). For example, investigators have suggested that cement lines are not traversed by collagen fibers and represent the weakest material in bone, and some have suggested that this explains the observation that microcracks tend to follow cement lines rather than crossing osteons or interstitial lamellae (Weidenreich, 1930; Maj and Toajari, 1937; Dempster and Coleman, 1961; Evans and Bang, 1966; Schaffler et al., 1995; Wang and Norman, 1996; Norman and Wang, 1997; Boyce et al., 1998; Jepsen et al., 1999). In turn, it has also been suggested that cement lines have important functions in other aspects of bone biomechanics, including fracture processes, energy absorption, elastic properties, and viscous damping (Dempster and Coleman, 1961; Piekarski, 1970; Lakes and Katz, 1974; Carter and Hayes, 1977; Saha, 1977; Lakes and Saha, 1979; Gottesman and Hashin, 1980; Katz, 1981; Martin and Burr, 1982; Burr et al., 1985; Choi and Goldstein, 1992; Norman et al., 1995; Guo et al., 1998; Currey, 2002; Les et al., 2004). In a given bone cortex, all of these functions have been considered to be influenced by the relative degree of mineralization and differences in the composition of cement lines, and their associated physical interfaces, with respect to immediately surrounding bone. Experimental data showing that cement line regions are enriched with noncollagenous proteins (e.g., osteocalcin, osteopontin, and bone sialoprotein) and other biochemical factors also suggest that, in addition to having important local adhesive and modulus mismatch functions, these narrow seams may also contain molecules that promote osteoclast-osteoblast coupling during bone remodeling and thereby help to maintain bone homeostasis and biomechanical integrity (e.g., influencing microdamage propagation and arrest, and localization for their repair) (Frasca et al., 1981b; Mundy et al., 1982; Baron et al., 1984; Parfitt, 1984; Hauschka et al., 1986; Ingram et al., 1993; Kagayama et al., 1993; McKee and Nanci, 1995, 1996a; Hosseini et al., 2000; Everts et al., 2002; Sit et al., 2003).

The description of highly mineralized cement lines has been challenged by biomechanical and compositional investigations (Fawns and Landells, 1953; Lakes and Katz, 1979; Lakes and Saha, 1979; Katz, 1980; Frasca, 1981; Frasca et al., 1981a; Lakes, 1995). For example, Frasca et al. (1981a) reported that increased numbers of secondary osteons in human compact bone specimens tested in shear resulted in reduced shear modulus and increased viscous behavior. They attributed these results to the possibility that cement lines of secondary osteons are more viscous than the surrounding bone, which, if true, may have allowed movement at interfaces formed between cement lines and immediately adjacent bone. This hypothesis, however, was not quantitatively examined at the microscopic level and may also be confounded by the use of only one cortical bone specimen from the tibia of a skeletally immature (12-year-old) human (Currey, 1984: p. 46–47; Parks and Lakes, 1986; Mabrey and Fitch, 1989). Computational analyses of Katz (1980), using a two-level hierarchical fiber-reinforced composite model, include the stiffness of the cement line surrounding secondary osteons in the effective modulus of interstitial lamellar bone, which the author assumed is one-quarter as stiff as secondary osteon bone tissue. Lakes and Saha (1979), observing displacements at the cement line in hydrated specimens subjected to a prolonged torsional load, concluded that the cement line is relatively more viscous than surrounding bone. Lakes and Saha (1979), however, referred to "cement lines" in plexiform bone (a primary, nonsecondary osteon, bone type) of the diaphyses of bovine limb long bones. Currey and Zioupos (Currey, 1984: p. 47, 2002: p. 80; Zioupos and Currey, 1994) have argued that these structures are not homologues of the cement lines of secondary bone, such as those observed around secondary osteons, the latter being those that some previous investigators have described as being relatively highly mineralized (Amprino and Engström, 1952; Jowsey, 1960, 1964, 1966; Philipson, 1965; Heuck, 1971; Lacroix, 1971; Yaeger, 1971). (Currey's argument is controversial in the context of nomenclature used by some investigators, who use the term "cement line" in descriptions of primary bone microstructure; see Appendix.)

Burr et al. (1988) and Schaffler et al. (1987) have also challenged the conception of the cement line as a highly mineralized entity. However, in contrast to previous investigations conducted a decade earlier, these investigators specifically analyzed cement lines at the classically defined anatomical locale: the outermost boundary of secondary osteons. Based on quantitative scanning electron microprobe analyses and qualitative observations of gray-level contrast in backscattered electron (BSE) images of cortical bone from adult human radii, they concluded that the cement lines are relatively poorly mineralized when compared to immediately adjacent bone (compare Fig. 2A and Fig. 3). This is an important finding not only because it refutes conventional histological and microradiographic descriptions noted above, but also because these and other authors are using these data to describe the influences of cement lines on the mechanical behavior and fracture mechanics of bone at the microstructural and macrostructural levels (e.g., Francillon-Vieillot et al., 1990; Hogan,

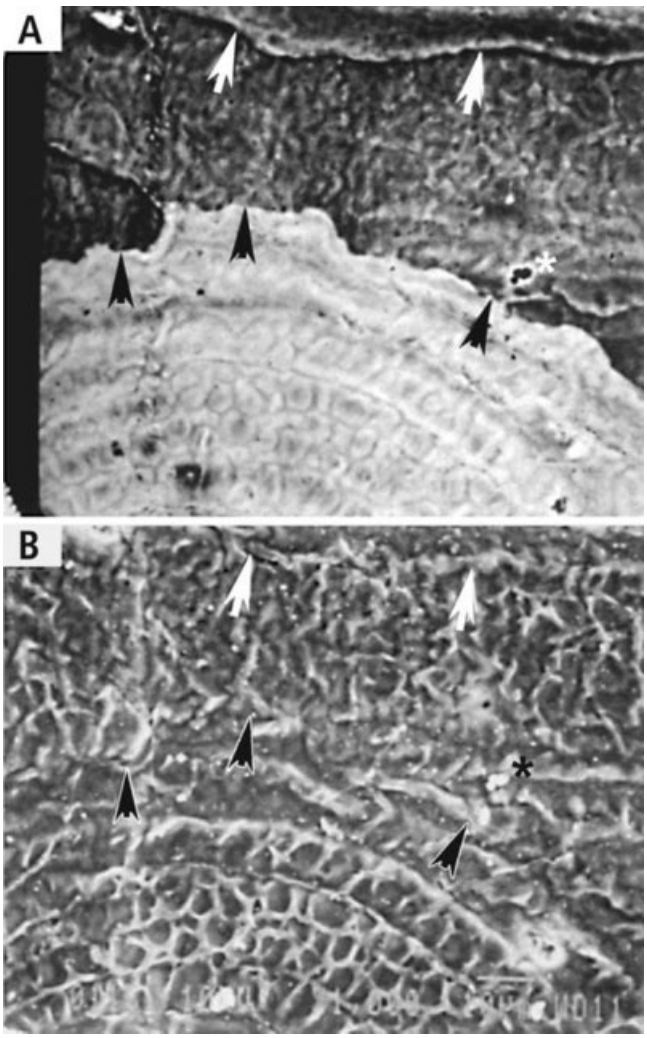

Fig. 3. Two microscopic images from Burr et al. (1988). **A:** Backscattered electron image showing two osteons. **B:** Secondary electron image of the same region. The same images also appear in Figure 2-21A of Martin and Burr (1989: p. 51). The original legend for these two images reads: "Backscattered and secondary electron images of osteonal cement lines (arrows). A: Backscattered electron image (1,000×) showing two cement lines from adjacent osteons. The osteon at the bottom of the micrograph is much more highly mineralized than the one at the top and is probably much younger. Note the cement line is a region of lower mass density even when compared to a young, incompletely mineralized osteon. B: Secondary electron image (1,000×) of the same region as in A demonstrates that cement lines are topographically indistinct." We speculate that in image A the polarity inadvertently was inverted, where higher atomic number materials have lower (darker), rather than higher (brighter), gray levels. This is suggested both by the designation of the lower, more highly mineralized osteon as "younger" and by the contrasts associated with the speck of debris near the dark arrowhead at the lower right of both images (marked with our asterisk). This debris, while presumably topographically higher than the surrounding specimen surface, shows unexpected contrast (i.e., a paradoxical dark gray level and bright halo). Images reproduced with permission by Elsevier.

1992; Zioupos and Currey, 1994; Norman et al., 1995; Courtney et al., 1996; Prendergast and Huiskes, 1996; Ascenzi et al., 1997; Yeni et al., 1997; Bosshardt et al., 1998; Clark and Stechschulte, 1998; Guo et al., 1998; Nanci, 1999; Rho et al., 1999; Brunski et al., 2000; Donahue et al., 2000; Muir and Ruaux-Mason, 2000; Phelps et al., 2000; Guo, 2001; Lakes, 2001; Nicolella et al., 2001; Frank et al., 2002; Sit et al., 2003; Dong and Guo, 2004; Les et al., 2004; Sobelman et al., 2004). If these data are truly representative of cement line mineralization, and because these data are at variance with the conventional interpretation of the highly mineralized cement lines seen in microradiographs, then novel explanations are warranted for the role of cement lines in the composite material properties of bone.

However, contrary to the observations of Burr et al. (1988), Boyde et al. (Boyde et al., 1990; Boyde and Jones, 1996; Boyde and Kingsmill, 1998; Howell and Boyde, 1999) have reported observing bright cement lines in BSE images of cortical and cancellous bone. Other investigators have also published BSE images of bone showing similarly bright cement lines (Dorlot et al., 1986; Roschger et al., 1993, 1997; Grynpas et al., 1994; Fratzl et al., 1996; Cool et al., 2002). In our laboratory, we have also seen bright lines coincident with the location of cement lines in BSE images of both cortical and cancellous bone (Bachus and Bloebaum, 1992; Bloebaum et al., 1997; Vajda et al., 1999). In these BSE images, the cement lines are not only relatively brighter than surrounding bone, but also closely resemble the dramatic contrast of bright cement lines in relatively darker surrounding bone seen in microradiographs of some previous studies (Amprino and Engström, 1952; Philipson, 1965; Lacroix, 1971; Yeager, 1971). Experimental studies have clearly demonstrated that relatively brighter gray levels in BSE images of bone represent relatively increased mineral content (w/w or v/v) and density (g/cc) (Reid and Boyde, 1987; Skedros et al., 1993a, 1993b; Roschger et al., 1995; Bloebaum et al., 1997). The conflicting nature of these independent observations with reports that suggest a hypomineralized cement line provided the impetus for the present study and review.

The present study uses advanced techniques to test the hypothesis that cement lines at the periphery of secondary osteons in the diaphyseal cortices of adult human long bones are relatively poorly mineralized relative to immediately surrounding bone. The techniques employed include quantitative energy dispersive X-ray (EDX) spectroscopy and quantitative atomic number contrast BSE imaging. Comparative observations were also made between light microscopic images and BSE images of the same fields of specimens treated with various stains showing uptake in the region of the cement line. Two additional goals of this study are to examine critically microanalysis methodologies in selected previous investigations, suggesting why our findings fundamentally differ from those reported in these previous investigations, and to consider implications of these disparate observations in a historical perspective of investigations that have considered cement line mineralization and/or composition as important for understanding bone biomechanics and remodeling dynamics.

MATERIALS AND METHODS

Specimen Preparation and Processing

Eight femora and five radii were obtained from adult human males and females with no evidence or history of skeletal pathology, diseases, or medication use that may have affected the metabolism or mechanical competence of the skeletal system (Table 1). Standard bone banking

TABLE 1. List of bone specimens

Bone type	Sex	Age
Radius	Female	18
Radius	Female	19
Radius	Male	34
Radius	Male	61
Radius	Male	69
Femur	Female	25
Femur	Female	34
Femur	Female	44
Femur	Female	44
Femur	Female	59
Femur	Male	50
Femur	Male	61
Femur	Male	80

procedures were used to obtain the bones (Bloebaum et al., 1993). All bones were dissected free of periosteum and other soft tissues. They were then stored in 70% ethyl alcohol for at least 2 months. Two 5 mm thick transversely cut segments were obtained from the mid-diaphysis of each bone. In the femora, these segments were between 40% and 50% of diaphyseal biomechanical length as defined by the osteometric axis system of Ruff and Hayes (1983).

A fragment of bone measuring 6 mm (radii) or 10 mm (femora) in mediolateral breadth was cut from the anterior cortex of one of the segments and subsequently cut into three smaller pieces of equal size. The centrally located piece was embedded in polymethyl methacrylate (PMMA) according to established protocols (Emmanuel et al., 1987), and the remaining two pieces were ashed to determine mineral content. Pairs of the embedded pieces were glued together with cyanoacrylate to form two-specimen aggregates that could be accommodated by the stage in the scanning electron microscope (SEM).

From six (three femora and three radii) of the original specimens, one additional cortical piece was obtained from the second transversely cut segment, adjacent to those that had been embedded in PMMA. These additional pieces were not embedded, but were dried for several months over anhydrous $CaSO_4$ (Drierite, W.A. Hammond Drierite, Xenia, OH) and placed in fast-drying epoxy. These unembedded and undemineralized samples were used to compare microscopic data or observations with results of Schaffler et al. (1987) and Burr et al. (1988) that were made using unembedded and undemineralized cortical bone.

In order to form a stable construct for imaging, each specimen aggregate was glued with a fast-drying epoxy resin into a well that had been milled into a Plexiglas block. The unembedded dried bone pieces were subsequently placed into vertical drill holes adjacent to the embedded pieces in one of the specimen aggregates. Fast-drying epoxy was used to anchor peripherally the dried unembedded specimens into the drill holes. Microscopic evaluation showed that with this technique the glue did not penetrate into the deeper locations of the specimens, where the microscopic analyses were conducted.

Additional drill holes were also made in the surface of each specimen block. Wires used for BSE image gray-level calibration standards (Vajda et al., 1995) were coated with epoxy and inserted into these drill holes. These wires included 99.8% pure magnesium-aluminum-zinc alloy (93% Mg, 6% Al, 1% Zi) and 99.9999% pure aluminum (Johnson Mathey, Seabrook, NH). Both blocks containing bone pieces and metal standards were then milled, ground, and polished with a buffing wheel to achieve an optical scratch-free finish (Bloebaum et al., 1990) on the surface that was coplanar with the anatomical transverse plane in which the bone segments were originally cut. The two polished specimen blocks were then lightly sputter-coated with gold for 60 sec at 70 μm Hg and 10 mA (Hummer Model VI-A Sputtering System, Anatech, Alexandria, VA). The presence or absence of PMMA embedding medium and the presence of the gold conductive coating used in the present study each has minimal influence on the accuracy of BSE gray-level interpretation and wt % Ca values obtained in quantitative EDX analysis of bone (Vajda et al., 1998). Additionally, studies conducted in our laboratory (data not shown) demonstrate that, using the methods described in the present study, no significant electron channeling contrast occurs ($< 1\%$ change in BSE gray level) when using these metal calibration standards in the manner described below.

Backscattered Electron Imaging

The BSE image measurements made in this study quantify specific mineralization (mineral per unit volume of bone tissue, excluding porosity) expressed as a percentage by weight (w/w) (Roschger et al., 1995; Bloebaum et al., 1997).

Specimens were imaged using the BSE mode of an SEM, with beam parameters at 20 keV accelerating voltage, 0.75 nA probe current, and 15 mm working distance. Backscattered electrons were collected by a four-quadrant annular-ring semiconductor BSE detector (Tetra, Oxford Instruments, Cambridge, U.K.) that was configured around the electron beam. BSE images were captured and digitized by a computer-controlled image capture and analysis system for analysis at a later time (eXL, Oxford Instruments).

In order to increase the signal-to-noise ratio, BSE images were captured using nine Kalman scans. SEM/BSE calibration procedures were conducted on the metal standards using 1,500× magnification according to the methods of Vajda et al. (1995). Consistent BSE/SEM operating conditions were maintained with computer control of brightness, contrast, objective lens strength, and condenser lens strength. A probe current detector (SM-16100 probe current detector, Jeol) connected to a picoammeter (model 485 Keithly Instruments, Cleveland, OH) was monitored between image collections. This allowed for a consistent probe current to within $\pm$ 0.001 nA; deviations were corrected by manual adjustments of the condenser lens.

Using methods of Vajda et al. (1995), weighted mean gray levels (WMGLs) of selected regions were calculated using a public domain software package using the public domain NIH image (v1.61) software (http://rsb.info.nih.gov/nih-image/). The analyzed gray-level spectrum ranged from 6 to 256; gray levels 0–5 were excluded for the purpose of eliminating the contribution of tissue voids (Bloebaum et al., 1997). Regional variations in weighted mean gray levels indicate relative differences in mean atomic number, which directly correlate with regional variations in mineral content in bone (typically, higher

WMGL = more mineralized) (Skedros et al., 1993a, 1993b; Vajda et al., 1998, 1999).

BSE image gray-level analysis was conducted on five complete secondary osteons that were randomly selected from each of the 13 PMMA-embedded and six unembedded cortical specimens. For both BSE and EDX images, the secondary osteons were selected randomly using a grid placed over the computer screen while viewing the field at low magnification. Grid boxes were numbered, and each measured 8 mm × 8 mm. Grid boxes were randomly selected using a random-number generator. Each osteon selected using this procedure was complete and exhibited the classical histological criteria described by Skedros et al. (1994). The selected osteons represented 10–20% of the osteons in the sectioned radial and femoral cortical fragments, and retrospective observation demonstrated that they were representative of the entire cross-section.

Within each selected osteon, the analyzed locations were also randomly chosen to minimize potential selection bias and intraosteonal variation. A template resembling a clock face with 10 radial locations was placed over each osteon under higher magnification. A random-number generator was used to identify each location for analysis; this method also served to eliminate selection bias of a bright or dark line at the osteon periphery (additional measures used to reduce selection bias are described below).

A region comprising a cement line and adjacent osteonal and interstitial bone (identified by localizing the crenulated margin of the secondary osteon) was imaged once at 1,500×, with the diameter of the analysis region being six pixels (approximately 0.7 μm^2). Interstitial bone was typically secondary osteons or secondary osteon fragments. In order to preclude selection bias further, the analyses were conducted in regions selected with respect to the crenulated interface corresponding to the reversal surface, irrespective of the presence or absence of a bright or dark line. Strict adherence to this protocol, ignoring a bright or dark line, if present, and conducting analyses with respect to the reversal surface, would eliminate such bias. Therefore, BSE gray-level analyses were conducted in five mutually exclusive sites at each of three osteon locations. Pilot studies comparing three to six sampling locations showed that three intraosteon locations adequately represented the variation in the cement line around the perimeter of the entire osteon. As shown in Figure 4, the five imaged sites at each of these osteon locations include the following: nearby interstitial secondary bone outside of the secondary osteon, with analysis region centered between 10 and 15 μm from the interstitial bone margin of the reversal surface; peripheral margin of the secondary osteon, defined by its morphological appearance (a crenulated surface at the periphery of the secondary osteon); peripheral osteonal bone, centered 0.7 μm from site 2; peripheral osteonal bone, centered 1.4 μm from site 2 (not overlapping site 3); and nearby osteonal bone, with analysis region centered between 10 and 15 μm from site 2.

Analysis of sites 2, 3, and 4 sampled the traditionally defined cement line region. WMGLs were calculated from the pixel gray-level data that were obtained from each of the five sites. One image at each site (five sites) at each location (three locations/osteon) was captured in random sequence in order to minimize the potential effects of bleaching (i.e., specimen degradation) that can occur during BSE image capture of bone tissue (Vajda et al., 1995, 1998). After imaging of each osteon for BSE or EDX analyses, the entire osteon was examined to determine if the bright line was present around the entire circumference of the osteon.

Energy Dispersive X-Ray Analysis

Quantitative EDX analysis was conducted on seven complete secondary osteons that were randomly selected from each of the embedded and unembedded cortical specimens. Beam positioning was achieved by viewing a BSE image at 4,000× magnification to ensure placement on the reversal interface. For each osteon, EDX analysis was performed at two osteonal locations and four sites (at each location) that were examined in random sequence (Fig. 4; site 3 was not sampled in the EDX analyses): nearby interstitial secondary bone outside of the secondary osteon, with analysis region centered between 10 and 15 μm from the interstitial bone margin of the reversal surface; peripheral margin of the secondary osteon, defined by its morphological appearance (a crenulated surface at the periphery of the secondary osteon); peripheral osteonal bone, centered 1.4 μm from site 2 (not overlapping site 2); and nearby osteonal bone, with analysis region centered between 10–15 μm from site 2.

The location equivalent to site 3 in the BSE imaging was not imaged here because the EDX interaction volumes are too large to resolve differences between sites 2 and 3, or sites 3 and 4 used in the BSE analyses.

EDX data were collected with a lithium-drifted silicon EDX detector (Pentafet, Oxford Instruments) equipped with a beryllium window and compiled for analysis by the Link eXL system. Spectra were collected during a 130-sec live sample period using 20 keV accelerating voltage and 35° takeoff angle; 99.99% pure calcium carbonate ($CaCO_3$) and indium phosphide (InP) were used as reference standards (Tousimis Research, Rockville, MD) and all data were quantified with commercially available ZAF correction (ZAF-4, Oxford Instruments) to account for atomic number (Z), absorption (A), and fluorescence (F) effects. The weight percent concentration of calcium (wt % Ca) was analyzed, while the light elements H, C, N, and O were characterized as nonanalyzed elements and were calculated with C selected as the dominant matrix element in accordance with ZAF correction methods described by Roschger et al. (1995). The Kα line of copper was used for gain calibrations. Pilot studies conducted in our laboratory have demonstrated that measurements of wt % *P* are not as reliable as wt % Ca, which is consistent with results published in other laboratories (Payne and Cromey, 1990; Åkesson et al., 1994). This may be the result of differences in irradiation mass loss between calcium and phosphorous (Edie and Glick, 1979) and/or the result of preparation methods preferentially leaching phosphorous from the bone tissue (Nicholson and Dempster, 1980). Therefore, only wt % Ca values are reported.

Percent Ash Content Analysis

The cortical pieces located immediately adjacent to the imaged specimens were ashed to determine mineral content (Skedros et al., 1993b). Mineral content (% ash) was determined by dividing the weight of the ashed bone (W_{ab}) by the weight of the dried defatted bone (W_{db}) and multiplying this number by 100 [(W_{ab}/W_{db}) X 100]. This was done in order to ensure that all bones were within a normal range of mineralization.

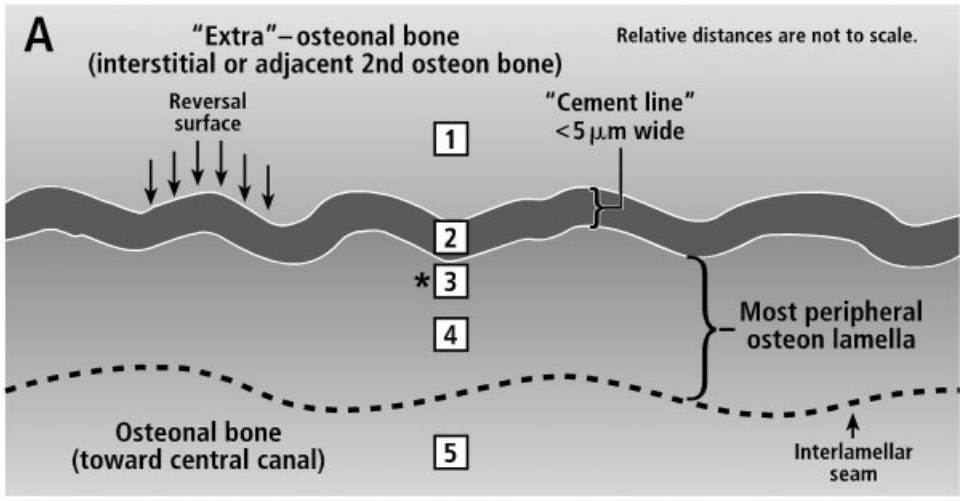

1 Nearby interstitial bone, 10-15μm from the interstitial margin of the "cement line."
2 Center of the "cement line".
3 Peripheral osteonal bone, 0.7μm from the osteonal margin of the "cement line" (* was not used in EDX analysis).
4 Peripheral osteonal bone, 1.4μm from the osteonal margin of the "cement line."
5 Nearby osteonal bone, 10-15μm from the osteonal margin of the "cement line."

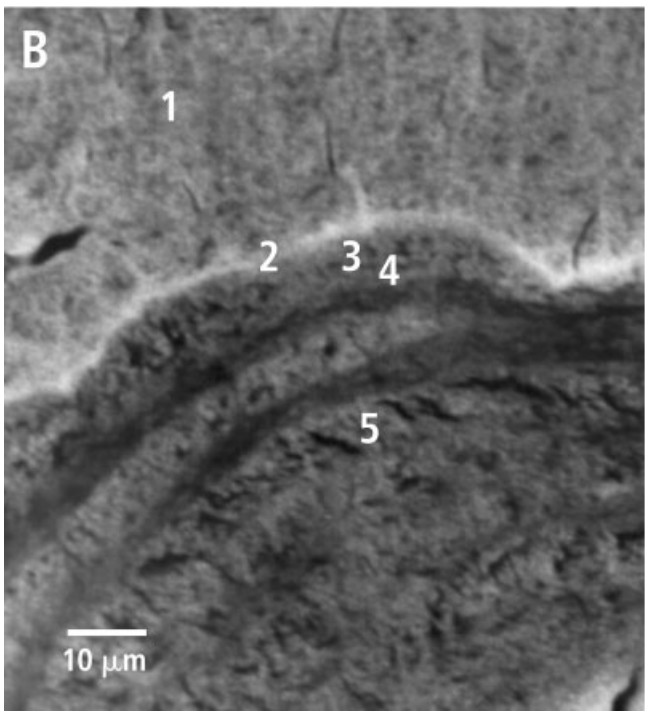

Fig. 4. **A:** Diagrammatic representation of the sites analyzed for atomic number contrast (gray levels) using quantitative calibrated backscattered electron imaging. Quantitative wt % Ca measurements made using EDX did not sample site 3. Site 2 is depicted as a dark line, consistent with the hypothesis that it is relatively hypomineralized with respect to immediately surrounding bone. It is plausible that site 3 may be the region of relatively hypomineralization described by Burr et al. (1988) as the cement line. **B:** Backscattered electron image at high magnification showing sites where the quantitative analyses were performed.

Correlated BSE and Light Microscopic Evaluations of Stained Sections

Three stains were used to observe cement lines: methylene blue buffered with potassium biphthalate (Nyssen-Behets et al., 1994), basic fuchsin and methylene blue mixture (Bain et al., 1990), and Villanueva (Villanueva et al., 1986). The stains were applied on thin ultramilled sections (40 microns) of undemineralized PMMA-embedded bone after BSE images were obtained from several

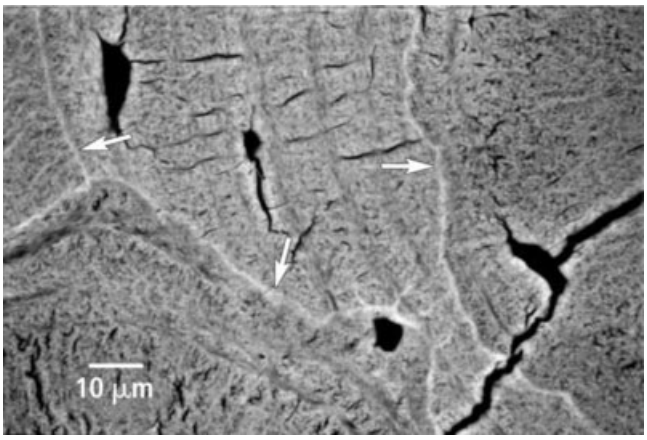

Fig. 5. Backscattered electron image (1,000×) of adult human femoral cortical bone (undemineralized and PMMA-embedded; transverse section, anterior cortex, mid-diaphysis). Classically defined cement lines are crenulated in appearance. The bright lines (arrows) in this image are consistent with this definition.

locations of the same sections. After BSE images were obtained, the specimens were first lightly polished with cloth to remove gold coating (used for BSE imaging), stained with one stain, and then imaged in a light microscope (Nikon HFX-IIA, Japan) using equivalent magnification. Finally, the regions were reimaged in the BSE mode of the SEM to determine what effect the stain had on local gray-level contrast.

Statistical Analysis

A two-way analysis of variance (ANOVA) design (intraosteonal site, embedment type) was used for all statistical analyses. The Fisher's PLSD posthoc test was used to determine significant differences ($P < 0.05$) between paired comparisons. This statistical approach is based on the fact that WMGL and EDX data have equivalent amounts of intra- and intersubject variance. Consequently, each osteon is viewed as being sufficiently unique to be included as an independent data source, and multiple measurements from a single osteon are considered as repeating factors.

RESULTS

Representative BSE images of cement lines and adjacent bone are shown in Figures 5 and 6. Quantitative results are listed in Tables 2 and 3, and embedded vs. unembedded BSE image gray-level data are summarized graphically in Figure 7. Unless otherwise stated, results are reported as mean ± SE (standard error). Results of the two-way ANOVAs did not reveal significant interactive effects between intraosteonal analysis sites and embedment type ($F = 1.342$; $P = 0.252$).

Backscattered Electron Image Weighted Mean Gray-Level (WMGL) Data

The BSE images shown in Figures 5 and 6 demonstrate that site 2, at the peripheral margin of secondary osteons, is coincident with a line (a thin seam of material < 5 μm wide) that has distinctly brighter gray level than the adjacent bone ($P < 0.01$); this bright line appears to be immediately adjacent to the reversal surface. Without exception, all secondary osteons observed during BSE imaging exhibited these bright lines (i.e., bright with respect to osteonal bone at sites 3, 4, and 5) at site 2, and these lines were continuous around the circumference of each osteon that was analyzed (including those examined for EDX analyses).

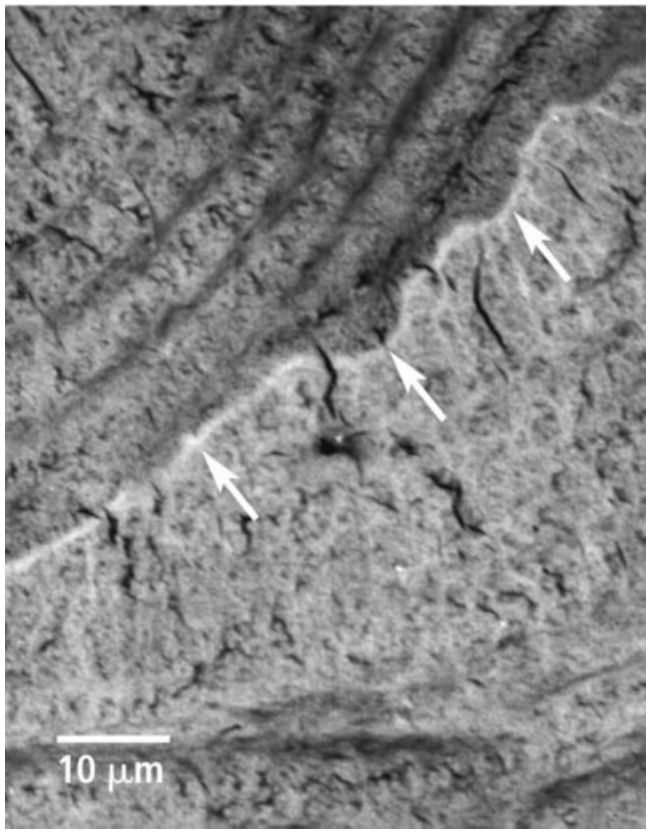

Fig. 6. Backscattered electron image (1,500×) of adult human femoral cortical bone (undemineralized and PMMA-embedded; transverse section, anterior cortex, mid-diaphysis; also see Fig. 4B). At top is a secondary osteon. At bottom is interstitial bone, which is relatively brighter than the osteon. The cement line region exhibits a thin seam of relatively bright material (arrows).

The average WMGL of site 2 in embedded specimens (109.1 ± 1.5) was significantly ($P < 0.01$) greater than the average WMGL of sites 3 and 4 (site 3: 65.7 ± 1.4; site 4: 56.8 ± 1.5). The average WMGL of site 2 was also greater than the average WMGL of site 1 (nearby interstitial bone, 74.2 ± 1.6; $P < 0.01$; Table 2). Average WMGLs of sites 1 and 2 were each greater than the average WMGL of site 5 (osteonal bone 10–15 μm from site 2, 64.7 ± 1.5; $P < 0.01$). In all possible comparisons, there were no significant differences in WMGL between sites 3 and 4 (the two measurements taken within 2 μm of the osteonal margin of the reversal line) and the osteonal bone at site 5 ($P > 0.15$).

Data in unembedded specimens showed relative regional average WMGL differences that are similar to the embedded specimens (Table 2, Fig. 7). Average WMGLs of regions in the unembedded specimens, however, were higher than average WMGLs of corresponding regions in embedded specimens.

TABLE 2. BSE gray-level results separated by embedment procedure (means ± standard errors)*

Site	PMMA	Unembedded	*P* value, PMMA vs. unembedded
Interstitial (site 1)	74.2 ± 1.6[b–e]	92.9 ± 2.4[b,d,e,g]	<0.01
Cement line (site 2)	109.1 ± 1.5[a,c–e]	127.8 ± 2.6[a,c–e]	<0.05
Site 3	65.7 ± 1.4[a,b,d,f]	87.5 ± 2.4[b,d,e,g]	<0.01
Site 4	56.8 ± 1.5[a,b,c,e]	76.5 ± 2.3[a–c,g]	<0.01
Osteonal (site 5)	64.7 ± 1.5[a,b,d,f]	77.9 ± 2.2[a–c,g]	<0.05

*WMGL, weighted mean gray level, where a higher numerical value represents higher atomic number (presumably higher mineral content).
[a]Significantly different ((*P* < 0.01) from site 1.
[b]Significantly different (*P* < 0.01) from site 2.
[c]Significantly different (*P* < 0.01) from site 3.
[d]Significantly different (*P* < 0.01) from site 4.
[e]Significantly different (*P* < 0.01) from site 5.
[f]For site 3 vs. 5: *P* > 0.5.
[g]For site 1 vs. 3, and 4 vs. 5: *P* > 0.1.

TABLE 3. EDX weight % calcium separated by embedment procedure (means ± standard errors)

Site	PMMA	Unembedded	*P* value PMMA vs. unembedded
Interstitial (site 1)	25.11 ± 0.44[d,e]	23.68 ± 0.58	NS
Cement line (site 2)	25.13 ± 0.46[c,d]	24.18 ± 0.81[f]	NS
Site 4	23.82 ± 0.49[b,e]	22.88 ± 0.56[f]	NS
Osteonal (site 5)	24.14 ± 0.38[a,b]	22.34 ± 0.74	NS

[a]Significantly different (*P* < 0.05) from site 1.
[b]Significantly different (*P* < 0.05) from site 2.
[c]Significantly different (*P* < 0.05) from site 4.
[d]Significantly different (*P* < 0.05) from site 5.
[e]For 1 vs. 4: *P* = 0.06.
[f]For 2 vs. 4: *P* = 0.08; 1 vs. 4: *P* = 0.18; 2 vs. 4: *P* = 0.16. All other nonsignificant site-to-site comparisons: *P* > 0.5.

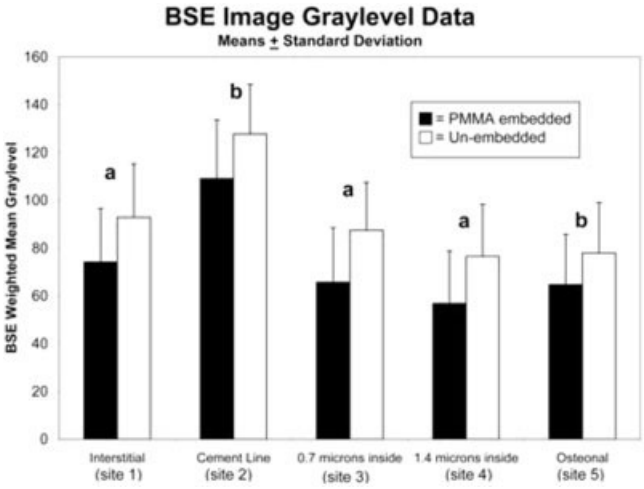

Fig. 7. Histogram doublets comparing backscattered electron image gray-level data of embedded vs. unembedded specimens. Statistically significant differences for each doublet are indicated (a, $P \leq 0.01$; b, $P \leq 0.05$). Statistical differences between the five sites are indicated in Table 2.

Energy Dispersive X-Ray Analysis Wt % Ca Data

In embedded specimens, average wt % Ca of site 2 (25.13 ± 0.46) was equivalent to the average wt % Ca of site 1 (nearby interstitial bone, 25.11 ± 0.44; $P > 0.5$). Average wt % Ca of both sites 1 and 2 were each greater than the average wt % Ca of sites 4 and 5 ($P \leq 0.06$; Table 3). There was no significant difference in wt % Ca between site 4 and 5 (the osteonal bone 10–15 μm from the margin of the reversal interface; $P > 0.5$).

In unembedded specimens, the relative regional wt % Ca differences are similar to the embedded specimens, but with two notable inconsistencies: average wt % Ca values of regions in the unembedded specimens tended to be lower than average wt % Ca values of all corresponding regions in embedded specimens, and there were statistical trends or tendencies for the following comparisons: site 2 vs. site 4 ($P = 0.08$) and site 2 vs. site 5 ($P = 0.15$).

Variations in WMGL and EDX Data

In approximately 90% of cases, the patterns of variations in EDX and BSE data among the five sites within any individual osteon (mean of three locations) were similar between all osteons examined. Specific differences at each location are detailed below.

In the 285 locations (195 in embedded and 90 in unembedded bones) that were sampled in the BSE WMGL analyses, there were no instances where site 2 was darker (i.e., had apparent lower mineralization) than sites 3, 4, and 5. There were 22 instances (7.7%) where site 2 was darker than the nearby interstitial bone (site 1), 120 instances (42.1%) where site 1 was darker than site 3, 72 instances (25.3%) where site 1 was darker than site 4, and 95 instances (33.3%) where site 1 was darker than site 5.

In the 266 locations (182 in embedded and 84 in unembedded bones) that were sampled in the EDX analyses, there

were 52 instances (19.6%) where site 2 had lower wt % Ca than the nearby interstitial bone (site 1), and 46 instances (17.3%) where site 2 had lower wt % Ca than site 4.

Ash Content Data

Ash percent data from bulk specimens ranged from 68.0% to 71.5%. This range is consistent with mature nonpathological human cortical bone (Trotter and Hixon, 1974). Pearson correlation coefficients (r values) determined in all possible comparisons between percent ash and regional WMGL, EDX-determined wt % Ca, or chronological age of the PMMA-embedded specimens (n = 13) were all < 0.23 (all P values greater than 0.19).

Analysis of Stained Sections

Figures 8–10 illustrate light microscopic images of classic-appearing cement lines in undemineralized human cortical bone with various stains. BSE images of the same fields demonstrate the topographic correspondence of cement lines with the bright lines seen in the present study.

DISCUSSION

Two plausible conclusions can be drawn from the present study. The quantitative BSE image data clearly indicate a zone of highly mineralized (or alternatively collagen-deficient) tissue. These data also demonstrate a region of possibly hypomineralized tissue 1.4 μm from the osteon periphery (toward the central canal), suggesting a two-phase mineralization zone. This hypomineralized zone was, however, only statistically significant in embedded bone tissue. In turn, the EDX data clearly reveal the absence of consistent significant regional wt % calcium differences. Hence, the EDX data suggest that there is no hyper- or hypomineralized zone at the periphery of secondary osteons. However, the discrepancy between the two analysis techniques may indicate the resolution limits of the EDX data, reflecting the sampling of relatively large interaction volumes that extend beyond the narrow limits of the target material. Although we used random sampling of relatively distant regions and a relatively lower-energy electron beam, 20 keV, in contrast to the 60 keV beam used by Burr et al. (1988), large sampling volumes are inevitable in EDX analysis (Table 4). Consequently, the comparatively greater resolution and stability of BSE image analysis may be the only accurate microprobe technique employed in the present study. Using either technique, however, our data contradict previous observations of hypomineralized cement lines.

Results of the quantitative BSE image analyses conducted in this study are consistent with numerous historical observations that cement lines of secondary osteons are coincident with a thin seam of material that is apparently more highly mineralized than immediately surrounding bone (Amprino and Engström, 1952; Jowsey, 1960, 1964, 1966; Smith, 1963; Philipson, 1965; Heuck, 1971; Lacroix, 1971; Yaeger, 1971; Pankovich et al., 1974; Dhem and Robert, 1986; Nyssen-Behets et al., 1994). For example, based on microradiographs of thin sections of femur and rib bone from adult orangutan and whale, respectively, Philipson (1965) provided evidence that cement lines are associated with highly mineralized material. Consistent with the images of Philipson (1965) and other recent investigators who have published BSE or microradiographic images of bone (Dorlot et al., 1986; Heuck, 1993; Grynpas et al., 1994; Boyde and Jones, 1996; Fratzl et al., 1996; Roschger et al., 1997; Boyde and Kingsmill, 1998; Howell and Boyde, 1999; Boivin and Meunier, 2002; Cool et al., 2002), the BSE images in this study demonstrate gray-level contrasts that are consistent with the interpretation that cement lines appear relatively highly mineralized. But, as discussed below, the possibility that cement lines may be relatively collagen-deficient appears to be a more parsimonious explanation for the regional variations in atomic number contrast.

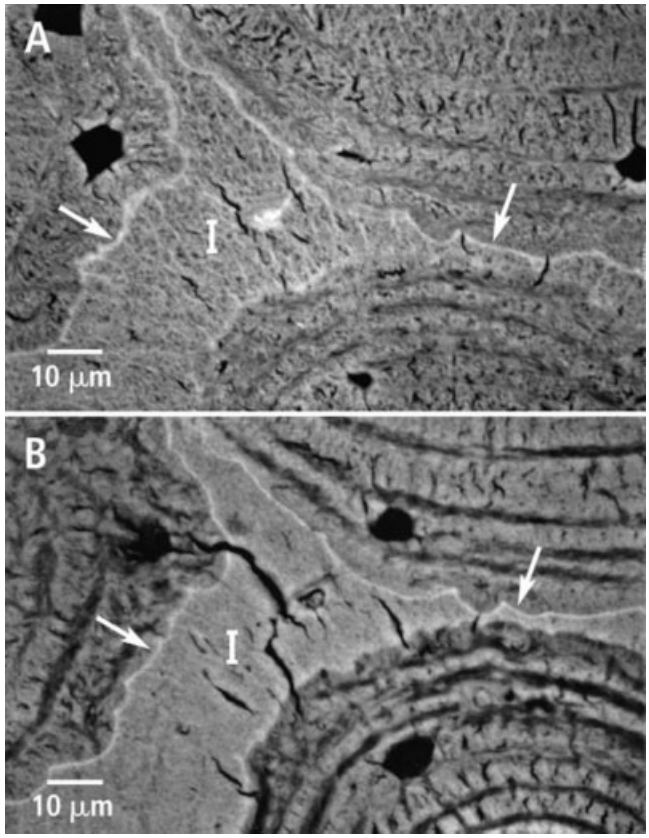

Fig. 8. Backscattered electron images (1,250×) of adult human femoral cortical bone (undemineralized and PMMA-embedded; transverse section, anterior cortex, mid-diaphysis). Portions of secondary osteons surrounding interstitial bone (I) are shown. **A:** Unstained bone tissue; this shows bright lines (arrows) and osteon lamellar morphology. Differences in contrast between the osteons and the enclosed interstitial bone suggest mineralization differences. **B:** The same region in A stained with methylene blue buffered with potassium biphthalate. The bright lines (arrows) are even more apparent than in the image in A, and greater uptake of the stain appears inside the osteons than in the interstitial bone, suggesting relatively increased collagen content (or less densely packed mineral).

Artifacts of Superimposition and Relatively Large Sampling Volumes

Burr et al. (1988) challenged the results of Philipson (1965) by arguing that the thickness (40–200 μm) of the latter's specimens could artifactually increase the brightness of the cement line by superimposing these lines over tissue of adjacent osteons and interstitial bone. The basis of this argument, however, appears invalid since it incor-

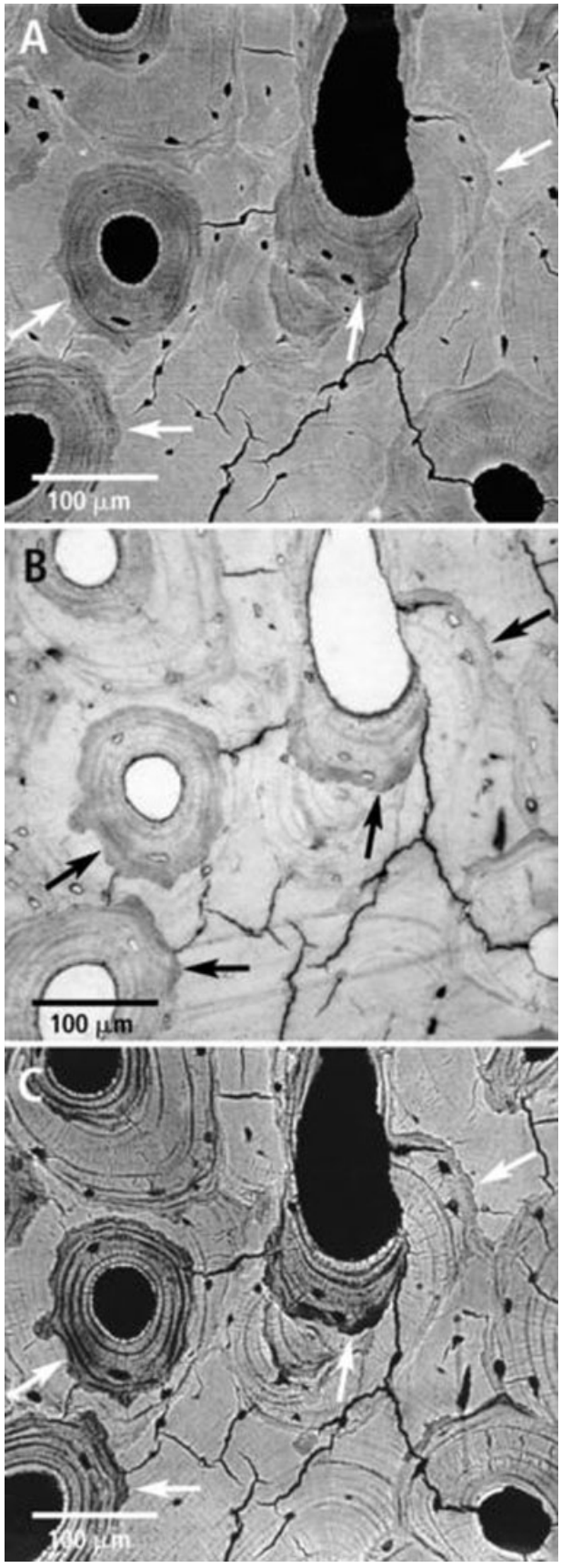

rectly predicts the effects of superimposition. If highly mineralized tissue were superimposed over less well mineralized tissue, then the net effect would be an image gray level with apparently intermediate mineralization with respect to the two superimposed materials. Therefore, if cement lines are relatively mineral-deficient, and if in microradiographic analysis they were superimposed by more highly mineralized adjacent tissue, then cement lines would likely be somewhat artificially brightened, but would still remain darker than surrounding tissue. We suggest, as have others (e.g., Sokoloff, 1973), that the superimposition of bone from adjacent secondary osteons and/or interstitial bone is a parsimonious explanation for the absence or variable presence of cement lines in microradiographs of human and nonhuman secondary osteon bone that have been published by several independent investigators (Amprino and Engström, 1952; Jowsey, 1960, 1964; Sissons et al., 1960; Sissons, 1962; Smith, 1963; Kornbulm and Kelly, 1964; Pankovich et al., 1974; Stout and Simmons, 1979; Dhem, 1980; Simmons, 1985; Zagba-Mongalima et al., 1988; Simmons et al., 1991; Bachus and Bloebaum, 1992; Nyssen-Behets et al., 1994; Meunier and Boivin, 1997).

A superimposition artifact could have influenced the data obtained from BSE image gray-level analyses as well as EDX microprobe analyses conducted in the present study, since the information obtained from these technologies is based on electron/X-ray interaction volumes that can sample tissue volumes exceeding the physical limits of a cement line (Murata, 1974; Goldstein et al., 1992: p. 69–147). However, BSE images and EDX analysis sample relatively minute tissue volumes, greatly reducing the superimposition artifact compared to microradiographs (Sumner et al., 1990; Bachus and Bloebaum, 1992; Roschger et al., 1995). Consequently, the use of both quantitative BSE and quantitative EDX techniques in the present study represents a major advance over previous studies that have used more limited technologies to address the same question.

Artifacts of Inadequate ZAF Correction and High-Energy Electron Beams

While Schaffler et al. (1987) and Burr et al. (1988) used BSE images only to illustrate cement lines, they also attempted to overcome the resolution limitations of microradiography by using EDX analysis. However, the unavailability of atomic number (Z), absorption (A), and fluorescence (F; ZAF) correction for data reduction restricted their ability to correct for the influence of bone matrix on X-ray generation. To reduce this error, these investigators used an internal standard ratio technique using intersti-

Fig. 9. Images of adult human femoral cortical bone (150×; undemineralized and PMMA-embedded; transverse section, anterior cortex, mid-diaphysis). The arrows indicate cement lines in each image. **A:** Backscattered electron image of unstained bone tissue to be used as a baseline for comparison. **B:** Transmitted light image of bone region in A stained with a basic fuchsin, methylene blue mixture. The regions of greatest stain uptake are just inside (i.e., toward the osteon central canal) of the bright lines seen in image A. **C:** Backscattered electron image of stained bone tissue showing regions of increased uptake. The regions of greatest uptake are just inside bright lines that appear coincident with cement line locations.

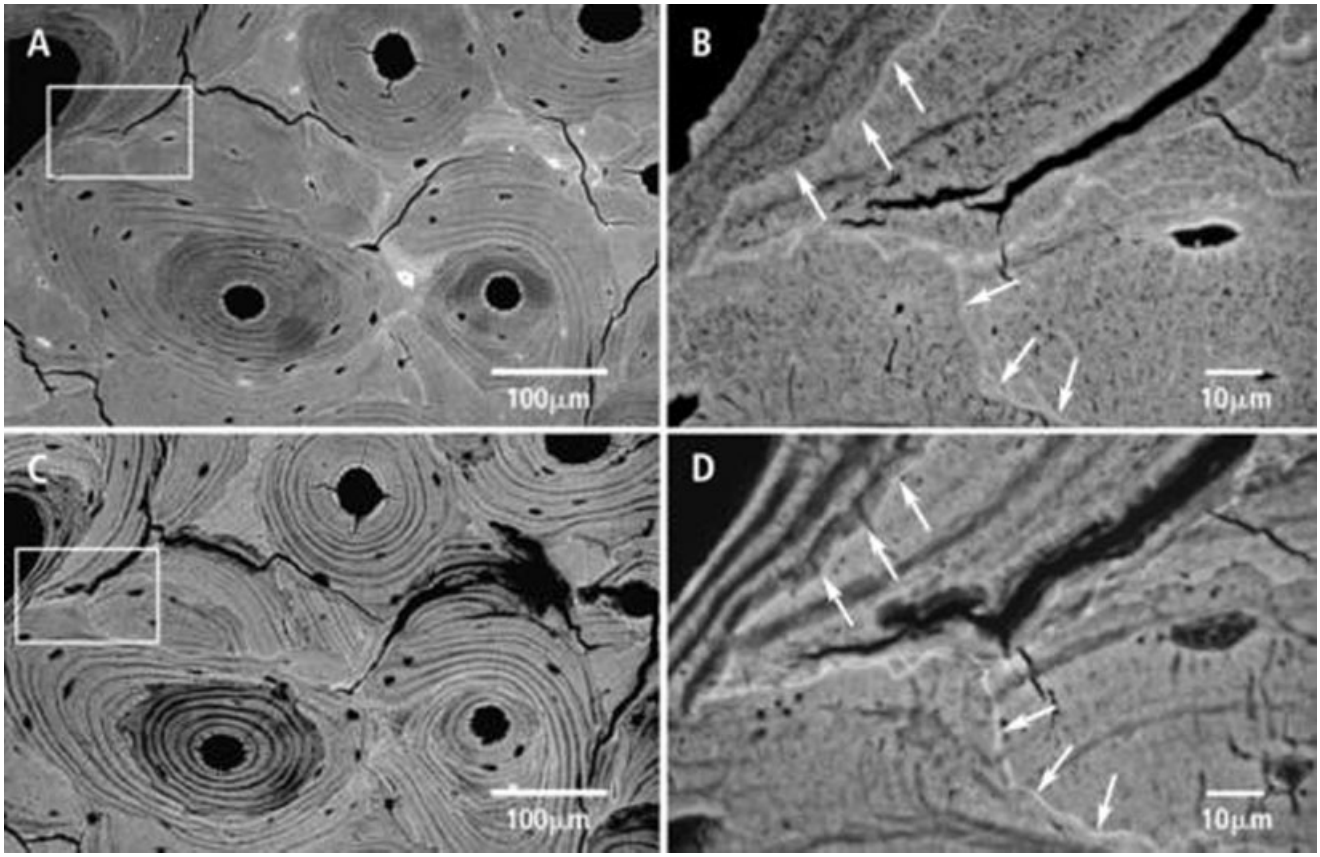

Fig. 10. Four backscattered electron images of adult human femoral bone (undemineralized and PMMA-embedded; transverse section, anterior cortex, mid-diaphysis). **A:** BSE image of unstained section with region of interest (170×). **B:** BSE image of unstained region in A at high magnification (350×); arrows show cement lines. **C:** BSE image of section in A stained with Villanueva stain, which is used to demonstrate cement lines with light microscopy (170×). **D:** BSE image of stained region in C at high magnification (350×); arrows show the same cement lines indicated in A. Stain uptake is greatest in interstitial bone outside the cement line. This accentuates the brightness of the cement line.

TABLE 4. Comparison of experimental conditions used in the present study vs. Schaffler et al. (1987)

Experimental conditions	Present study	Schaffler et al. (1987)
Accelerating voltage (kV)	20	60
Probe current	2.5 nA	20 μA[a]
X-ray collection time (sec)	75	60
Magnification	4,000	4,000
Correction method	ZAF	Internal standard
Processing	Unembedded, hand-polished, or ultramilled	Unembedded, hand-polished
Coating material	Gold	Carbon

[a]Emission current value given instead of probe current value.

tial bone as the standard. Notably, this technique assumes that the matrix composition is equivalent between the internal standard and all of the sampled regions. Their data, however, suggest that the mineral and nonmineral phases of the cement line are not compositionally equivalent to those of the immediately adjacent regions.

In contrast to the 20 keV electron beam used in the present study, these investigators also used a much higher accelerating voltage, 60 keV (Table 4). Because these higher-energy electrons would penetrate much deeper into the tissue, and probably a considerable distance beyond the physical limits of the target material, there could be a marked decrease in accuracy of the information obtained (Vajda et al., 1996; Wong and Elliott, 1997; Holmes et al., 2000). Although these previous authors claimed that the electron probe sampled to a depth of less than 5 microns and the volume of tissue sampled by the microprobe was well within the boundaries of the cement line, our calculations suggest that the range of X-ray generation is much larger. Even if the electron beam diameter is as small as 100 Ångströms, once the electrons interact with the specimen, a series of elastic and inelastic scattering events leads to a substantial broadening of the sampled region (Fig. 11). X-ray generation range can be

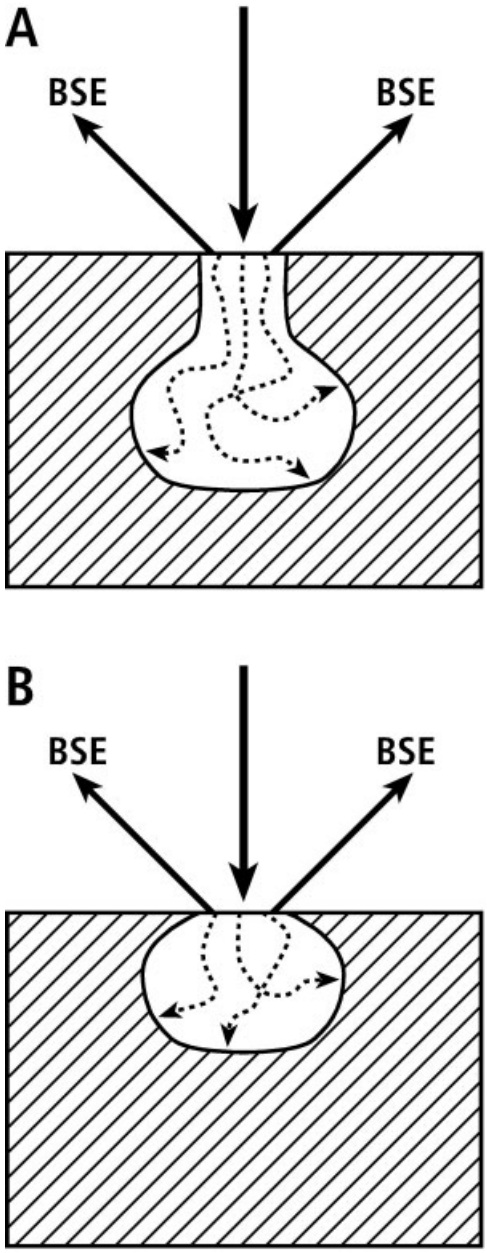

Fig. 11. Diagrammatic representations of electron range and interaction volume differences in a bulk material. BSE = backscattered electron. **A:** High electron beam energy or low Z leads to a large electron range. **B:** Low beam energy or high Z causes a decrease in electron range.

estimated using the Kanaya-Okayama (K-O) range (Kanaya and Okayama, 1972). This range can be calculated using a modified K-O equation (Goldstein et al., 1992: p. 89, 130–133):

$$R_{K\text{-}O} = \frac{0.0276A(E^{1.68} - E_c^{1.68})}{Z^{0.89}\rho}$$

where $R_{K\text{-}O}$ is X-ray range (μm), A is atomic weight, E is incident electron energy (keV), E_c is characteristic X-ray energy of desired element (keV), Z is atomic number, and ρ is density [g/cc; some of these values were obtained from Skedros et al. (1993b)]. This range of X-ray generation does not take into account X-rays generated from fluorescence effects and does not account for the fact that X-ray generation is not uniformly distributed (Murata, 1974). Nonetheless, this estimate emphasizes that the volume sampled using a 60 keV could exceed 35 μm (compared to < 10 μm in the present study). A large X-ray range can lead to decreased resolution, excessive absorption effects, and can violate the fundamental assumption of EDX analysis that the sampled region is homogeneous (Goldstein et al., 1992: p. 415–416). This may in part explain the contradiction between the findings of Schaffler et al. (1987) and Burr et al. (1988) and the data presented in this study and observations of previous investigators.

Although the interaction volume of EDX analysis limits the certainty that the sampled volume of tissue is confined to the desired region, this effect was reduced in the present study by the use of a relatively lower accelerating voltage (20 keV) (Holmes et al., 2000). The lower accelerating voltage also reduces the influence of excessive X-ray absorption. Furthermore, the use of ZAF corrections represents an advance over the techniques used in previous studies. However, the accuracy of absolute wt % values of elements obtained by EDX analysis of bulk biological specimens has recently been questioned (Payne and Cromey, 1990; Vajda et al., 1996, 1998). Conventional EDX does not directly measure low-energy X-rays generated by the light elements such as carbon and oxygen, and ZAF corrections may not adequately account for these variables. Despite these limitations, published experimental data demonstrate that EDX accurately measures relative differences in Ca content (Åkesson et al., 1994; Roschger et al., 1995; Vajda et al., 1996, 1998).

BSE Image Analysis: Advantages and Artifacts

ZAF corrections. Quantitative BSE analysis solves several of the inherent weaknesses of EDX analysis. There are no ZAF corrections to be performed in BSE analysis, and the interaction volume of incident electrons is substantially smaller than in EDX analysis (Goldstein et al., 1992: p. 69–147), increasing the likelihood that the sampled region resides within the cement line. Schaffler et al. (1987) and Burr et al. (1988) did not perform quantitative BSE analysis, making a direct comparison with the present study difficult. They did, however, report that the cement line "appeared consistently as a dark band between osteonal and interstitial lamellae" (Burr et al., 1988). Their BSE photomicrographs appear to support this statement. This is in stark contrast to the findings reported in the present study; in 285 observations of BSE images, the material of the cement line was never measured as being darker than the nearby osteonal bone. Additionally, only 42% (120/285) of the observations showed that site 3 [which may be the cement line sampled by Burr et al. (1988)] was darker than site 1 (interstitial bone). Based on qualitative observations, Boyde and Jones (1996: p. 117) have similarly reported "our BSE data contradict the view of Burr et al. (1988) that cement lines are normally less mineralized than the surrounding lamellar matrix." The smaller accelerating voltage and use of ZAF corrections in the present study may explain the discrepancy with respect to results of EDX analysis in the present study with previous studies (Schaffler et al., 1987; Burr et

al., 1988) and historical observations (Holmes et al., 2000), but does not explain the disparity between their qualitative observations in BSE images and the qualitative observations and quantitative BSE image data reported in the present study.

Image topography and aqueous vs. nonaqueous specimen preparation. Subtle surface topography visible in the secondary images corresponding to the BSE images of Burr et al. (1988) may have also contributed to variations in BSE signals near cement line regions (Howell and Boyde, 1994; Vajda et al., 1999). In theory, it is possible that local gray-level contrast in BSE images could be artificially affected by minute topography, even though this topography, when present, is only on the order of $< \pm$ 0.5 microns (Vajda et al., 1999). This is possible since topographic peaks and troughs can change effective electron interaction volumes and thereby alter the corresponding backscattered fraction of electrons collected by the BSE detector (Figs. 12 and 13) (Goldstein et al., 1992: p. 69–148; Howell and Boyde, 1994, 1999; Vajda et al., 1999). But recent quantitative experimental studies have shown that BSE image atomic number contrast associated with cement line regions cannot be the result of surface topography of ultramilled or polished specimens at nominal magnifications (e.g., 50–200×) (Howell and Boyde, 1999; Vajda et al., 1999). Topography may have a greater effect at the higher magnification used in the present study. However, the fact that the corroborative techniques used in the present study demonstrated cement lines with high atomic number contrast or, generally, regionally equivalent Ca content in several hundred independent samples essentially eliminates the possibility of significant artifacts attributable to topography.

Roschger et al. (1993) have also demonstrated that the use of water during grinding/polishing of undemineralized methacrylate-embedded bone, such as used in the present study, can produce ultracracks that are visible in magnifications from 1,000× to 3,000×. However, their BSE images demonstrate bright cement lines whether or not water was used during grinding and polishing procedures.

Effects of image magnification and tissue embedding techniques. Our published BSE images of cortical bone of calcanei of adult deer (Skedros et al., 1994, 2004), and radii and third metacarpals of adult horses (Mason et al., 1995; Skedros et al., 1996), do not consistently demonstrate obvious cement lines or gray-level contrasts in the vicinity of osteonal cement lines resembling the contrast seen in the human bones examined in the present study. Reasons for these discrepancies are clear; bright lines are consistently present if the images are viewed at higher magnifications (typically higher than 100×; data not shown).

Embedding media typically used by bone histologists can influence the results obtained by quantitative BSE images and EDX analysis by introducing a new material phase that can significantly affect electron interaction volumes and the relative absorption of X-rays (Payne and Cromey, 1990; Wong and Elliott, 1997). Although the absolute wt % Ca and WMGL values varied between embedded and unembedded specimens examined in the present study, the same pattern of regional differences was generally observed with both methods of specimen preparation. EDX analyses showed that in both cases, the bright

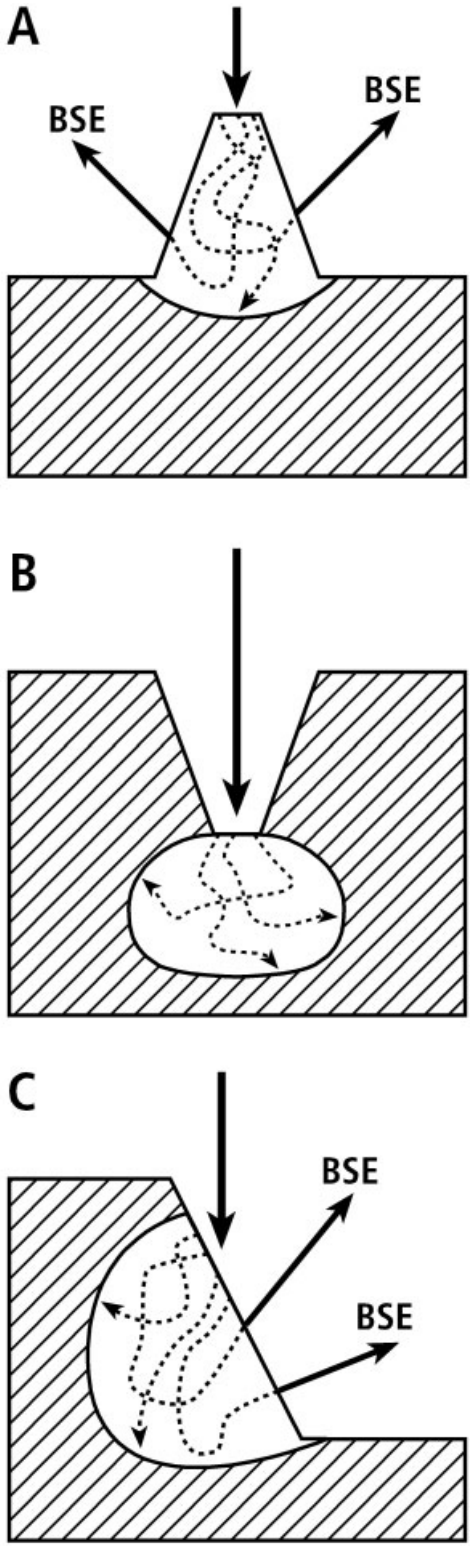

Fig. 12. Electron scattering from topographic peaks (**A**), troughs (**B**), and edges (**C**) of a bulk material. The large vertical arrow in each drawing represents the incident electron beam. Greater fractions of backscattered electrons (BSEs, smaller arrows) cause peaks and edges to appear brighter than troughs.

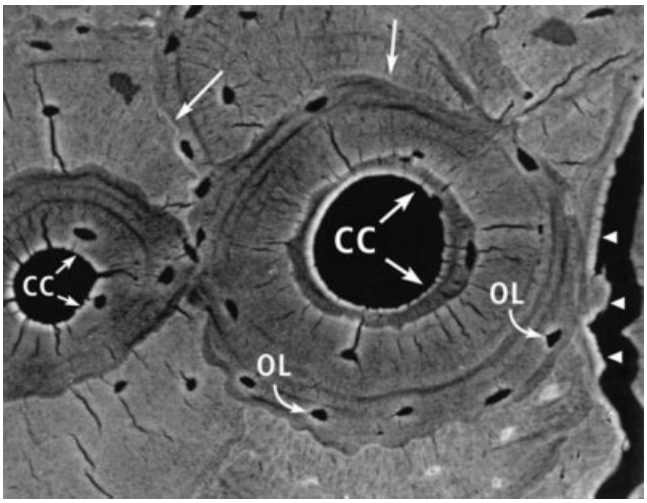

Fig. 13. Backscattered electron image (200×) of adult human femoral bone (undemineralized and PMMA-embedded; transverse section, anterior cortex, mid-diaphysis). The cement line regions exhibit a distinctly bright line (two white arrows in top third of image). This image demonstrates how brightness can be enhanced at edges. This is typically attributed to topography between the embedding material and target material. e.g., at margins of central canals (CC, arrows) or cracks in the bone (arrowheads at far right). However, in some locations, the brightness along the edges may be influenced by tissue composition or organization, e.g., the surfaces of osteocyte lacunae (OL, curved arrows) (Vose and Baylink, 1970; Marotti, 1996). Therefore, correlated topographic and quantitative analyses are needed to ensure that significant topography is not present. We have conducted such experiments in our laboratory and have concluded that topography in PMMA-embedded cortical bone specimens prepared using the methods described in the present study cannot explain the stark gray-level contrasts in the cement line region (Vajda et al., 1999).

lines (site 2) typically were more similarly mineralized (i.e., had similar Ca content) compared to surrounding bone tissue. This negates the possibility that the discrepancy between the current study and that of Schaffler et al. (1987) and Burr et al. (1988) (where unembedded specimens were used) is an artifact due to the specimen embedment.

Bone embedment in resins, such as PMMA, typically requires aqueous fixation. Fixation in some solutions (e.g., EDTA or formalin) can contribute to demineralizing the tissue and/or translocating molecules (e.g., noncollagenous proteins) from one location to another (Nicholson et al., 1977; Landis and Glimcher, 1978; Frasca et al., 1981b). However, significant demineralization or translocation is not known to occur with common alcohol fixation protocols used in the present study. Translocation of mineral, occurring in vivo as a result of diffusion and convective flow, has also been suggested as an explanation for the relative hypermineralization of central vs. peripheral lamellae of secondary osteons (Martin, 1993). But this does not explain the apparent hypermineralization of cement lines suggested by the BSE analyses in the present study since relatively young secondary osteons (darker gray levels in BSE images) also have these bright lines (Grynpas et al., 1994). However, results of in vitro experiments suggest that the translocation of noncollagenous proteins (e.g., bone sialoprotein) may account for relative differences in their relative concentrations between peripheral and central portions of secondary osteons (Hosseini et al., 2000). Alternatively, relative differences in the protein synthetic and secretory capacity of differentiating osteogenic cells (which make the cement line) and already differentiated osteoblasts (which make the successive concentric lamellae) may account for these regional differences (see Appendix) (Marotti, 1996; Hosseini et al., 2000; Kato et al., 2001; Hofmann et al., 2003).

Effects of tissue age. Boyde and Jones (1996: p. 117) have observed that "aberrant, nonmineralized 'cement lines' may form in elderly bone. In younger individuals, all cement lines appear to have a higher mean atomic number (higher density)." We have also made similar observations (data not shown) in bone specimens from individuals of advanced age. Although careful inspection of each osteon examined in the present study did not reveal nonmineralized cement lines, a more rigorous analysis of all osteons in large areas of bone cortex would be necessary to conclude whether or not nonmineralized cement lines occur in our specimens.

Mineral-Enriched vs. Collagen-Deficient

In support of their conclusion that cement lines are relatively mineral-deficient with respect to surrounding bone, Schaffler et al. (1987) and Burr et al. (1988) noted that in a scanning electron microprobe study of cortical bone from human femora, Mellors (1964) was unable to demonstrate increased calcium or phosphorous in cement lines. However, Mellors (1964) did not report quantitative data dealing with cement lines, but merely included one graphic illustration of a linear traverse X-ray microprobe scan showing the Ca Kα line across the boundary of two adjacent secondary osteons. This illustration exhibits large variations that may have been substantially influenced by signal noise, which makes quantitative interpretation dubious at best.

In a study of the "deposition of cement at reversal lines in rat femoral bone," Zhou et al. (1994: p. 367) stated that "using phase-contrast optics and X-ray microscopy, respectively, cement lines have also been described as bands of reduced density." In support of this statement, these investigators reference the text by Weinmann and Sicher (1955) and book chapter by Jee (1983). Our perusal of the Weinmann and Sicher (1955) text, however, did not reveal any mention of the use of phase-contrast optics or X-ray microscopy. In fact, Weinmann and Sicher (1955: p. 46) stated that "in silver-impregnated sections the cement lines remain entirely unstained. Their strong basophilia is matched by complete argyrophobia. The lack of stainability in silver impregnation proves that these lines do not contain fibrils. They may consist of cementing substance only, which shows the same staining reactions of cementing lines."

Jee (1983) also did not mention or show the use of phase-contrast optics, but did include one microradiograph of bone obtained from Jowsey (Jee, 1983: p. 223). This microradiograph did not show relatively bright cement lines, which, as discussed above, might be attributable to superimposition artifact because a 200 micron thick section was used. Jee stated that "surrounding the outer border of each osteon is a 'cement line,' a 1–2 μm thick layer of mineralized matrix deficient in collagen fibers." The term "reduced density" and "deficient in col-

lagen" are not necessarily synonymous in this context (personal communication, W.S.S. Jee).

The possibility that cement lines at the periphery of secondary osteons are highly calcified and/or collagen-deficient with respect to surrounding bone, although not definitively established, can be critically considered in the context of the data reported in the present study. In a strict sense, the physical basis for the gray-level contrasts seen in BSE images of composite materials is dependent on corresponding atomic number variations in the target material (Skedros et al., 1993a, 1993b; Vajda et al., 1996, 1998; Bloebaum et al., 1997; Wong and Elliott, 1997). It is therefore possible that the bright lines seen in the present study are collagen-deficient rather than hypermineralized with respect to surrounding tissue. This interpretation has been suggested by previous investigators for traditional (secondary osteonal) cement lines, resting lines, and hypermineralized lamellae (Schmidt, 1959; Ortner and von Endt, 1971; Sokoloff, 1973; Frasca, 1981; Tran Van et al., 1982; Zhou et al., 1994; Skedros et al., 1995; Davies, 1996; Hosseini et al., 2000). Most of these suggestions were based on light microscope observations of thin sections of osteonal bone treated with various stains. As noted, use of the light microscope, in addition to superimposition artifact, may reduce the ability to discern what may be two zones at the interface of a secondary osteon and surrounding bone: the apparently hypermineralized line and immediately adjacent material of somewhat different composition.

Recent studies have shown that osteoclasts can resorb bone mineral just beyond the resorption surface (perhaps up to 1 or 2 microns) (Boyde and Jones, 1987; Zhou et al., 1994; Nesbitt and Horton, 1997; Salo et al., 1997). It had been suggested to us that this demineralized zone (organic material remains) along the resorption surface may subsequently become relatively highly mineralized (i.e., remineralized) with respect to surrounding bone and may be the bright line seen in the BSE images and microradiographs (personal communication, M.B. Schaffler). Although this interpretation seemed unlikely to us, we designed our experimental protocol to eliminate its potential influence prospectively on our data by specifically analyzing the cement line region at three locations (sites 2, 3, and 4 in Fig. 4) in the area of the reversal line, irrespective of the presence or absence of a bright line. Nevertheless, if a region of resorbed mineral subsequently becomes hypermineralized, it might not be readily possible to distinguish this region (also presumably scalloped in appearance) from the actual resorption surface using BSE imaging. Thus, the true resorption surface might best be thought of as a relatively broader zone.

It should be emphasized that the BSE and EDX measurements made in the present study refer to mineral content of the bone material as a weight fraction (wt mineral/wt bone) (Roschger et al., 1995, 1997; Bloebaum et al., 1997). Therefore, it is not always possible to discriminate between increased mineral content and decreased collagen content. The weight fraction relationship could be identical in either case, even if the volume fractions [and hence material density (g/cc)] are different. Previous investigators (Weidenreich, 1930; Schmidt, 1959; Ortner and von Endt, 1971; Sokoloff, 1973; Frasca, 1981; Zhou et al., 1994; Davies, 1996; Hosseini et al., 2000) have suggested that the cement lines and/or other cement line-like structures are collagen-deficient, and the data provided in the present study do not preclude this interpretation. This is not the same, however, as a "region of reduced mineralization" as described by Burr et al. (1988). In fact, the bright cement lines seen in the microradiograph in Figure 14 suggest relatively increased mineralization because the physical basis for the gray-level contrasts in such images is a direct relationship of X-ray absorption and the amount of Ca present (Amprino and Engström, 1952; Bachus and Bloebaum, 1992; Wong and Elliott, 1997).

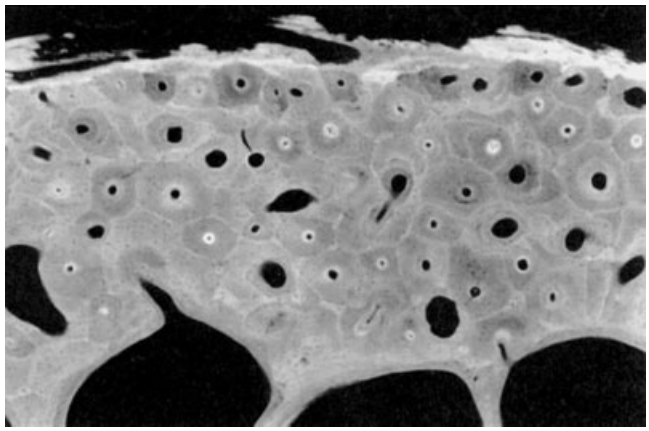

Fig. 14. Microradiograph of dog rib bone tissue showing relatively highly mineralized cement lines. Field width is approximately 2.5 mm.

Osteon Reversal Region and Evidence From Ultrastructural and Scanning Acoustic Microscopy (SAM) Studies

In a recent study using calvariae and metatarsals of 5-day-old mice, Everts et al. (2002) showed that bone lining cells deposit a layer of proline-rich protein at the bottom of cleaned Howship's lacunae. They suggest that this material, which contains osteopontin, "represents the so-called lamina limitans or cement line, which demarcates sites where formation of new bone is initiated." Their definition, however, may be too restrictive for the biomechanical and physiologic implications for the composition and structural interfaces formed by the material of the cement line region. We suggest that the composition of the cement line region may be heterogeneous, including the initial materials deposited by differentiating osteoblasts and bone lining cells [this role for this cell type is controversial (Mulari et al., 2004)]. Zhou et al. (1994) and Hosseini et al. (2000) have also described heterogeneity of the material constituents across the cement line region. Using young adult Widstar rats, they describe the cement line in forming secondary osteonal bone as having two zones: globular accretions (possibly proteoglycan) that are deposited onto the demineralized resorption surface, and new collagen fibers formed on the globular accretions, which subsequently mineralize. They noted that "the [new] globules increased in size and fused laterally to form a continuous cement layer, which not only interdigitated with the collagen mesh of the resorption surface but also provided anchorage for new collagen fibers, which themselves became mineralized" (Zhou et al., 1994: p. 367).

We speculate that, by the time the osteon matures, the globular region becomes apparently hypermineralized

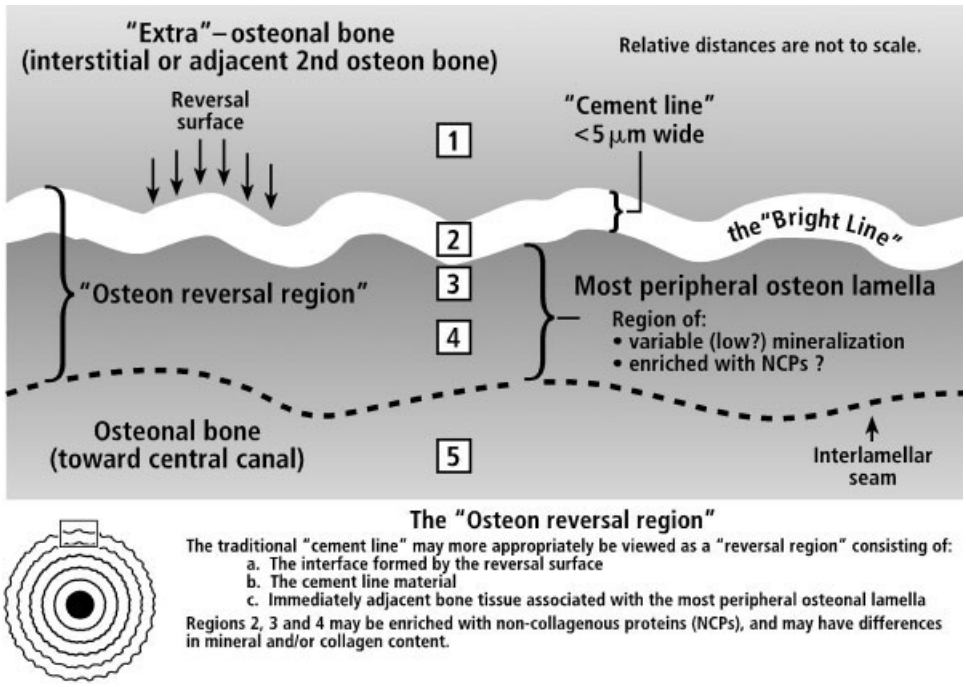

Fig. 15. Diagrammatic depiction of the osteon reversal region concept.

with respect to immediately surrounding tissue. However, discretion must be exercised when extrapolating these data in mice and rats to results of the present study since these recent investigators do not report relative differences in the mineralization of these zones, and since these animals typically do not form secondary osteons. In addition to these issues, interspecies differences, where regions described as cement lines might not be homogeneous, may also limit comparisons with data reported in the present study (Currey, 1984, 2002; de Ricqlès et al., 1991).

We suggest that, because of its compositional heterogeneity, the traditional cement line region (at the peripheral margins of secondary osteons) may be more appropriately described as the osteon reversal region (Fig. 15). This region is characterized by (1) the interface formed by the reversal surface and the cement (reversal) line; (2) the cement line, that is, the material shown to be immediately adjacent to the reversal surface, to be a bright line in BSE images, to have Ca content similar to nearby bone tissue by EDX analysis, and possibly to be enriched with noncollagenous proteins (Schaffler et al., 1987; Burr et al., 1988; Ingram et al., 1993; McKee and Nanci, 1996a; Hosseini et al., 2000); and (3) the tissue adjacent to the cement line (toward the central canal in the vicinity of site 4) that may have relatively lower mineralization than deeper (site 5) osteonal bone, and which could also be relatively enriched with noncollagenous proteins (Ingram et al., 1993; Hosseini et al., 2000) and may have lamellar organization that differs from other deeper lamellae (Martin et al., 1996; Hiller et al., 2003). If this interpretation is correct, then it is possible that the load-induced viscous behavior of osteonal bone that is attributed to the cement line/region and/or its interface in secondary osteonal bone (Hogan, 1992; Prendergast and Huiskes, 1996) may in part reflect different elastic moduli and adhesive/attachment properties of these specific material constituents across the entire osteon reversal region.

The concept of the osteon reversal region, however, is not consistent with the SAM images published by Katz and Meunier (1993), which do not show a notable change in elastic modulus in the vicinity of cement lines of secondary osteons in canine and human femoral bone. A. Meunier (personal communication) suggested to us that this unexpected finding might be attributable to relative collagen deficiency of the cement line, making highly mineralized cement lines in a BSE image appear to have equivalent elastic modulus (with respect to immediately adjacent bone) in their SAM images. This may be one among other plausible conditions where local composition and/or ultrastructure is sufficiently heterogeneous to influence atomic number contrast, hence BSE image gray levels, in ways that are not expected (Vose and Baylink, 1970; Skedros et al., 1993a, 1993b; Wong and Elliot, 1997). Further studies are needed to investigate these possibilities. The SAM observations of Katz and Meunier (1993) may also be confounded by lower resolution when compared to our BSE images (Meunier et al., 1988; Broz et al., 1995). The resolution using a 600 MHz transducer is about 3 μm and the volume sampled is proportional to this value (personal communication, A. Meunier). The SAM images are obtained in a reflection mode and the thickness of the specimen affected by the wave is two wavelengths (5 μm; personal communication, A. Meunier). Further investigation of the possibility that this resolution is not adequate for detecting the bright line seen in the present study is warranted. Additionally, further study of the physical basis of gray-level contrasts in SAM images is warranted since these contrasts have not been investigated with the experimental rigor that has been applied to

understanding gray levels in BSE images of bone, and this SAM technology may also be relatively more sensitive to topographic artifact (Bumrerraj and Katz, 2001).

Implications for Osteon Pullout

The "osteon reversal region" concept also helps explain more fully the results of osteon pullout studies. Scanning electron micrographs of pullout surfaces demonstrate that there is a zone where debonding occurs, and this is not discretely at the cement line (Piekarski, 1970, 1984; Behiri and Bonfield, 1980; Moyle and Bowden, 1984; Corondan and Haworth, 1986; Bonfield, 1987; Braidotti et al., 1997; Hiller et al., 2003). The region of pullout appears to extend across a broader area that includes the cement line and several of the most peripheral osteonal lamellae. For example, Braidotti et al. (1997) used scanning electron microscopy to study failure surfaces of undecalcified samples of human femoral diaphyses fractured in bending. They found evidence of some cement line fragments in the fracture surfaces. Additionally, their micrographs clearly revealed broken calcified collagen fiber bundles of various lengths protruding above the fracture surfaces across a broad area of the osteonal wall in both dry and wet samples. These observations suggest that a broader zone of the osteon periphery contributes to failure resistance by increasing energy absorption capacity. It is hypothesized that these broader pullout regions are attributable at least in part to the material heterogeneity such as shown in the present study and in these previous studies, consistent with the "osteon reversal region" concept.

Ultrastructural/histocompositional modifications that modify pullout of secondary osteons can improve local (e.g., within a cortical region) stiffness, strength, fatigue resistance, and energy absorption (work of fracture) (Hiller et al., 2003). Since pullout occurs when the tensile strength of osteons exceeds the shear strength (Martin et al., 1998), modifications in the osteon reversal region can contribute in modifying shear strength in this context. Tissue enhancements that in theory could correlate with pullout strength include mineralization of the cement line and mineralization variations across the cement line interface; ultrastructure and composition of the cement line; adhesion/attachment of the cement line to surrounding tissue; osteon diameter; and lamellar organization at the osteon periphery [e.g., predominantly highly oblique-to-transverse collagen orientation in peripheral lamellae of the "hoop" osteons described by Martin et al. (1996)], and composition of the peripheral lamellae (e.g., enriched with some noncollagenous proteins such as osteocalcin and osteopontin) (Moyle and Bowden, 1984; Schaffler et al., 1987; Burr et al., 1988; Martin and Burr, 1989; Hogan, 1992; Ingram et al., 1993; Martin et al., 1996; McKee and Nanci, 1996a; Hosseini et al., 2000; Hiller et al., 2003).

Mineral-Deficient vs. Hypermineralized: Historical Observations of Cement Line Composition and Mineralization, and Implications for Bone Biomechanics and Remodeling Dynamics

Investigations into the composition of the cement line have often been motivated by desire to better understand the remodeling process. For example, the initial material(s) deposited on the reversal surface is known to be important for enabling the attachment of osteoblasts (McKee and Nanci, 1996a; Everts et al., 2002; Mulari et al., 2004). These materials appear to be noncollagenous proteins (e.g., osteocalcin, osteopontin, bone sialoprotein), some of which are correlated with the subsequent initiation and/or degree of cement line mineralization (Hunter and Goldberg, 1993; McKee and Nanci, 1995, 1996b; Davies, 1996; Hunter et al., 1996; Tye et al., 2003; Pampena et al., 2004; Xiao et al., 2004). In addition, some of these proteins have been correlated with osteoclastic recruitment and activation. It is hypothesized that normal fatigue-related microdamage (e.g., microcracks) could be an event that causes this release/exposure in the cement line region. In turn, osteoclastic activity could further expose or release these proteins, thus further stimulating osteoclast recruitment and/or activity. Although there are observations and data that indirectly support these possibilities (Von Ebner, 1875; Baron et al., 1984; Hauschka et al., 1986; Hauschka and Wians, 1989; Glowacki et al., 1991; Denhardt and Guo, 1993; Ingram et al., 1993; Gerstenfield, 1999; Terai et al., 1999; Zhu et al., 2001), additional studies aimed at testing these hypotheses are needed.

As noted earlier, studies of cement lines have also often been motivated by a desire to understand the mechanical consequences of the interface formed at the cement line and the adhesive/attachment properties of this interface. But it could be argued that either a hypo- or hypermineralized cement line can achieve the mechanically beneficial stiffness differences across the vicinity of the cement line. In view of the above discussion and implications of the present study, however, this emphasis on the mechanical roles of cement line interfaces should not overshadow the importance of the myriad functions that cement line ultrastructural/histocompositional enhancements (i.e., compared to nearby bone tissue) have in the biomechanics and remodeling dynamics involving this region. For example, purely mechanical considerations reveal little about the potential variations in cellular activities and protein synthesis during early stages of osteon formation. Compositional and ultrastructural heterogeneities of the osteon periphery might reflect spatiotemporal changes in the biosynthetic capacities that differentiating osteogenic cells undergo as they transition from osteoblasts to osteocytes (Marotti, 1996; Hosseini et al., 2000; Kato et al., 2001; Hofmann et al., 2003). Using computer-aided reconstruction of transmission electron micrographs of bone tissue, Marotti et al. (1996) provide data that support this idea. These investigators describe three types of preosteocytes, which are distinguishable by cell position and shape, ultrastructure of the tissue surrounding the cell, and rate of tissue deposition. In view of these designations, the differentiating osteogenic cells responsible for cement line deposition are closely associated with the successive series of cells that can produce biomechanically important variations in osteon lamellar organization (Marotti, 1996; Martin et al., 1996), which can influence the viscoelastic behavior of bone (Hiller et al., 2003). Further studies of the capacities that differentiating osteogenic cells, osteoblasts, and preosteocytes have in modifying cement line mineralization or composition, and/or the organization of the closely associated peripheral lamellae, might help explain causal bases for some viscoelastic behaviors of compact bone that have otherwise been difficult to define (for further discussions, see Currey, 2002; Hiller et al., 2003; Les et al., 2004).

Improved understanding of the regulation of the cellular activities involved in the formation of the heterogeneous osteon reversal region and of the bone subsequently deposited also has implications in the burgeoning field of endo-osseous implant fixation (Davies, 1996; Brunski et al., 2000). Skeletal fixation at bone/implant interfaces (e.g., hip replacements, screws, and Brånemark-type dental implants) appears to involve a series of steps that seem to mirror osteonal cement line formation. For example, in an article reviewing in vitro methods dealing with how new bone is formed on solid surfaces of implants, Davies (1996) noted that these methods "not only mimic in vivo phenomena, but also provide a mechanistic understanding of bone elaboration at implant surfaces." Although Davies's cement line designation encompasses nonosteonal bone, the possibility that the sequence of events in osteonal and nonosteonal cement line formation is highly similar warrants repeating a summary of his findings here since they strongly emphasize how detailed understanding of cement line composition, mineralization, and ultrastructure can have broad implications for basic and applied bone biology: "The sequence starts with secretion and adsorption to the [implant] substratum of organic components, of which the major proteins are osteopontin and bone sialoprotein. Mineralization of this matrix occurs by the seeding of nanocrystalline calcium phosphate, which precedes the appearance of morphologically identifiable collagen fibers. This is clearly contrary to the dogma that collagen is necessary for mineralization of bone, but is in agreement with specific cases of other, particularly dental, calcified connective tissues. Although collagen is synthesized by the differentiating osteogenic cells that elaborate the cement line interface, it is not adsorbed to the underlying solid surface. Following the elaboration of the cement line matrix, collagen fiber assembly occurs and is then mineralized to produce morphologically identifiable bone matrix" (Davies, 1996: p. 426).

Summary and Future Directions

The quantitative data reported in this investigation support previous studies that have suggested that cement lines of secondary osteons of adult human cortical bone are relatively highly mineralized (or collagen-deficient; BSE analyses) or similarly mineralized (EDX analyses) when compared to surrounding bone. These data therefore reject the hypothesis that the traditional secondary-osteon cement line is poorly mineralized with respect to immediately surrounding osteonal bone. The absence of apparent highly mineralized cement lines in microradiographs of human bone in several independent studies may be a consequence of superimposition artifact. In contrast to the term "cement line," the term "osteon reversal region" may be more appropriate for describing the structural and material organization, and the biomechanics of the complex composite interface that is formed after the reversal of bone resorption during remodeling.

Additional studies are needed to reevaluate and extend the scope of previous theoretical and experimental analyses of viscoelastic behavior of cortical bone that are based on the hypothesis of poorly mineralized cement lines in osteonal (Haversian) and fibrolamellar or other forms of nonosteonal bone. Although the results of these previous studies may accurately depict viscoelastic behavior of bone, the hypothesis that in tested specimens a substantial proportion of the matrix motion specifically occurs in the immediate vicinity of, or within, cement lines or cement line-like interfaces will require additional rigorous experimental analysis. It has been suggested that regardless of whether the cement line is conceived as highly mineralized, poorly mineralized, or collagen-deficient, all of these conceptions in theory could provide the point-specific stiffness differences, fiber-matrix bonding characteristics, and energy transfer qualities desirable in a fiber-reinforced composite subject to repeated loading. However, determining the chemical constituents that comprise the osteon reversal region is an important goal since they may influence the remodeling process.

ACKNOWLEDGMENTS

The authors thank Pierre Durand for technical work, anonymous reviewers for their suggestions, and R. Bruce Martin and Scott Sorenson for critiquing the manuscript. They also thank Mitch Schaffler and David Burr for addressing their questions and thereby helping them to advance the imaging techniques and protocol ultimately used in the study, and Scott Miller for providing the microradiograph of a dog rib.

LITERATURE CITED

Advani SH, Lee T-S, Martin RB. 1987. Analysis of crack arrest by cement lines in osteonal bone. In: Erdman AG, editor. Advances in bioengineering BED, vol. 3. New York: American Society of Mechanical Engineers. p 57–58.

Åkesson K, Grynpas MD, Hancock RG, Odselius R, Obrant KJ. 1994. Energy-dispersive X-ray microanalysis of the bone mineral content in human trabecular bone: a comparison with ICPES and neutron activation analysis. Calcif Tissue Int 55:236–239.

Amprino R, Engström A. 1952. Studies on X-ray absorption and diffraction of bone tissue. Acta Anat 15:1–22.

Ascenzi A, Ascenzi MG, Benvenuti A, Mango F. 1997. Pinching in longitudinal and alternate osteons during cyclic loading. J Biomech 30:689–695.

Bachus KN, Bloebaum RD. 1992. Projection effect errors in biomaterials and bone research. Cells Mater 2:347–355.

Bain SD, Impeduglia TM, Rubin CT. 1990. Cement line staining in undecalcified thin sections of cortical bone. Stain Technol 65:1–5.

Baron R, Vignery A, Horowitz M. 1984. Lymphocytes, macrophages and the regulation of bone remodeling. In: Peck WA, editor. Bone and mineral research, annual 2. Amsterdam: Elsevier. p 175–243.

Behiri JC, Bonfield W. 1980. Crack velocity dependence of longitudinal fracture in bone. J Mater Sci 15:1841–1849.

Bloebaum RD, Bachus KN, Boyce TM. 1990. Backscattered electron imaging: the role in calcified tissue and implant analysis. J Biomater Appl 5:56–85.

Bloebaum RD, Lauritzen RS, Skedros JG, Smith EF, Thomas KA, Bennett JT, Hofmann AA. 1993. Roentgenographic procedure for selecting proximal femur allograft for use in revision arthroplasty. J Arthroplasty 8:347–360.

Bloebaum RD, Skedros JG, Vajda EG, Bachus KN, Constantz BR. 1997. Determining mineral content variations in bone using backscattered electron imaging. Bone 20:485–490.

Boivin G, Meunier PJ. 2002. The degree of mineralization of bone tissue measured by computerized quantitative contact microradiography. Calcif Tissue Int 70:503–511.

Bonfield W. 1987. Advances in the fracture mechanics of cortical bone. J Biomech 20:1071–1081.

Bosshardt DD, Zalzal S, McKee MD, Nanci A. 1998. Developmental appearance and distribution of bone sialoprotein and osteopontin in human and rat cementum. Anat Rec 250:13–33.

Boyce TM, Fyhrie DP, Glotkowski MC, Radin EL, Schaffler MB. 1998. Damage type and strain mode associations in human compact bone bending fatigue. J Orthop Res 16:322–329.

Boyde A, Maconnachie, Reid SA, Delling G, Mundy GR. 1986. Scanning electron microscopy in bone pathology: review of methods, potential and applications. Scanning Electr Microsc 4:1537–1554.
Boyde A, Jones S. 1987. Early scanning electron microscopic studies of hard tissue resorption: their relation to current concepts reviewed. Scanning Microsc 1:369–381.
Boyde A, Hendel P, Hendel R, Maconnachie E, Jones SJ. 1990. Human cranial bone structure and the healing of cranial bone grafts: a study using backscattered electron imaging and confocal microscopy. Anat Embryol 181:235–251.
Boyde A, Jones SJ. 1996. Scanning electron microscopy of bone: instrument, specimen, and issues. Microsc Res Tech 33:92–120.
Boyde A, Kingsmill VJ. 1998. Mineralisation density of human mandibular bone: quantitative backscattered electron image analysis. J Anat 192:245–256.
Braidotti P, Branca FP, Stagni L. 1997. Scanning electron microscopy of human cortical bone failure surfaces. J Biomech 30:155–162.
Broz JJ, Simske SJ, Greenberg AR. 1995. Material and compositional properties of selectively demineralized cortical bone. J Biomech 28:13457–1368.
Brunski JB, Puleo DA, Nanci A. 2000. Biomaterials and biomechanics of oral and maxillofacial implants: Current status and future developments. Int J Oral Maxillofac Implants 15:15–46.
Bumrerraj S, Katz JL. 2001. Scanning acoustic microscopy study of human cortical and trabecular bone. Ann Biomed Eng 29:1034–1042.
Burr DB, Martin RB, Schaffler MB, Radin EL. 1985. Bone remodeling in response to in vivo fatigue microdamage. J Biomech 18:189–200.
Burr DB, Schaffler MB, Frederickson RG. 1988. Composition of the cement line and its possible mechanical role as a local interface in human compact bone. J Biomech 21:939–945.
Carter DR, Hayes WC. 1977. Compact bone fatigue damage: a microscopic examination. Clin Orthop 127:265–274.
Castanet J. 1981. Nouvelles donnees sur les lignes cimentates de l'os. Arch Biol (Bruxelles) 92:1–24.
Choi K, Goldstein SA. 1992. A comparison of the fatigue behavior of human trabecular and cortical bone tissue. J Biomech 25:1371–1381.
Clark J, Stechschulte DJ Jr. 1998. The interface between bone and tendon at an insertion site: a study of the quadriceps tendon insertion. J Anat 193:605–616.
Cool SM, Forwood MR, Campbell P, Bennett MB. 2002. Comparisons between bone and cementum compositions and the possible basis for their layered appearances. Bone 30:386–392.
Corondan G, Haworth WL. 1986. A fractographic study of human long bone. J Biomech 19:207–218.
Courtney AC, Hayes WC, Gibson LJ. 1996. Age-related differences in post-yield damage in human cortical bone. Experiment and model. J Biomech 29:1463–1471.
Currey JD. 1984. The mechanical adaptations of bones. Princeton, NJ: Princeton University Press.
Currey JD. 2002. Bones: structure and mechanics. Princeton, NJ: Princeton University Press.
Davies JE. 1996. In vitro modeling of the bone/implant interface. Anat Rec 245:426–445.
Dempster WT, Coleman RF. 1961. Tensile strength of bone along and across the grain. J Appl Physiol 16:355–360.
de Ricqlès A, Meunier FJ, Castanet J, Francillon-Vieillot H. 1991. Comparative microstructure of bone. In: Hall BK, editor. Bone, vol. 3. Boca Raton, FL: CRC Press. p 1–78.
Denhardt DT, Guo X. 1993. Osteopontin: a protein with diverse functions. FASEB J 7:1475–1482.
de Ricqlès A, Meunier FJ, Castanet J, Francillon-Vieillot H. 1991. Comparative microstructure of bone. In: Hall BK, editor. Bone, vol. 3. Boca Raton, FL: CRC Press. p 1–78.
Dhem A. 1980. Etude histologique et microradiographique des manifestations biologiques propres au tissu osseux compact. Bull Mem Acad R Med Belg 135:368–381.
Dhem A, Robert V. 1986. Morphology of bone tissue aging. In: Uthoff HK, Stahl E, editors. Current concept of bone fragility. Berlin: Springer-Verlag. p 363–370.
Donahue SW, Sharkey NA, Modanlou KA, Sequeira LN, Martin RB. 2000. Bone strain and microcracks at stress fracture sites in human metatarsals. Bone 27:827–833.
Dong XN, Guo XE. 2004. Geometric determinants to cement line debonding and osteonal lamellae failure in osteon pullout tests. J Biomechanical Eng 126:387–390.
Dorlot J-M, L'Esperance G, Meunier A. 1986. Characterization of single osteons: microhardness and mineral content. Trans 32nd Orthop Res Soc 11:330.
Edie JW, Glick PL. 1979. Irradiation effects in the electron microprobe quantitation of mineralized tissues. J Microsc 117:285–296.
Emmanual J, Hornbeck C, Bloebaum RD. 1987. A polymethyl methacrylate method for large specimens of mineralized bone with implants. Stain Technol 62:401–410.
Evans FG, Bang S. 1966. Physical and histological differences between human fibular and femoral compact bone. In: Evans FG, editor. Studies on the anatomy and function of bone and joints. New York: Springer. p 142–155.
Everts V, Delaissé, Korper W, Jansen DC, Tigchelaar-Gutter W, Saftig P, Beertsen W. 2002. The bone lining cell: its role in cleaning Howship's lacunae and initiating bone formation. J Bone Min Res 17:77–90.
Fawcett DW. 1994. Bloom and Fawcett: a textbook of histology, 12th ed. New York: Chapman and Hall. p 224.
Fawns HT, Landells JW. 1953. Histochemical studies of rheumatic conditions: I, observations on the fine structures of the matrix of normal bone and cartilage. Ann Rheum Dis 12:105–113.
Francillon-Vieillot H, de Buffrénil V, Castanet J, Géraudie J, Meunier FJ, Sire JY, Zylberberg L, de Ricqlès A. 1990. Microstructure and mineralization of vertebrate skeletal tissues, In: Carter JG, editor. Skeletal biomineralization: patterns, processes and evolutionary trends, vol. 1. New York: Van Nostrand Reinhold. p 471–530.
Frank JD, Ryan M, Kalscheur VL, Ruaux-Mason CP, Hozak RR, Muir P. 2002. Aging and accumulation of microdamage in canine bone. Bone 30:201–206.
Frasca P. 1981. Scanning-electron microscopy studies of "ground substance" in the cement lines, resting lines, hypercalcified rings and reversal lines of human cortical bone. Acta Anat 109:115–121.
Frasca P, Harper R, Katz JL. 1981a. Strain and frequency dependence of shear storage modulus for human single osteons and cortical bone microsamples: size and hydration effects. J Biomech 14:679–690.
Frasca P, Harper RA, Katz JL. 1981b. Scanning electron microscopy studies of collagen, mineral and ground substance in human cortical bone. Scanning Electr Microsc 3:338–346.
Fratzl P, Schreiber S, Roschger P, Lafage M-H, Rodan G, Kalushofer K. 1996. Effects of sodium fluoride and alendronate on the bone mineral in minipigs: a small-angle X-ray scattering and backscattered electron imaging study. J Bone Miner Res 11:248–253.
Frost HM. 1963. Bone remodeling dynamics. Springfield, IL: Charles C. Thomas.
Frost HM. 1973. Bone modeling and skeletal modeling errors. Springfield, IL: Charles C. Thomas.
Frost HM. 1990. Skeletal structural adaptations to mechanical usage (SATMU): 2, redefining Wolff's law: the remodeling problem. Anat Rec 226:414–422.
Gerstenfeld LC. 1999. Osteopontin in skeletal tissue homeostasis: an emerging picture of the autocrine/paracrine functions of the extracellular matrix. J Bone Miner Res 14:850–855.
Goldstein JI, Newbury DE, Echlin P, Joy DC, Romig AD Jr, Lyman CE, Fiori C, Lifshin E. 1992. Electron-specimen interactions. In: Scanning electron microscopy and x-ray microanalysis: a text for biologists, material scientists, and geologists. New York: Plenum Press. p 69–147.
Glowacki J, Rey C, Glimcher MJ, Cox KA, Lian J. 1991. A role for osteocalcin in osteoclast differentiation. J Cell Biochem 45:292–302.
Gottesman T, Hashin Z. 1980. Analysis of viscoelastic behavior of bones on the basis of microstructure. J Biomech 13:89–96.
Grynpas MD, Holmyard DP, Pritzker KPH. 1994. Bone mineralization and histomorphometry in biopsies of osteoporotic patients treated with fluoride. Cells Mater 4:287–297.
Guo XE, Liang LC, Goldstein SA. 1998. Micromechanics of osteonal cortical bone fracture. Trans ASME J Biomech Eng 120:112–117.
Guo XE. 2001. Mechanical properties of cortical bone and cancellous bone tissue. In: Cowin SC, editor. Bone mechanics handbook, 2nd ed. Boca Raton, FL: CRC Press. p 10.1–10.23.

Ham AW, Cormack DH. 1979. Histophysiology of cartilage, bone, and joints. Philadelphia: J.B. Lippincott. p 367–485.
Hauschka PV, Maviakos AD, Iafrati MD, Doleman SE, Klagsbrun M. 1986. Growth factors in bone matrix. J Biol Chem 261:2665–2674.
Heuck F. 1971. Investigations of high density areas in metabolic bone diseases. Isr J Med Sci 7:477–480.
Heuck FW. 1993. Comparative histological and microradiographic investigations of human bone. In: Grupe G, Garland AN, editors. Histology of ancient human bone: methods and diagnosis. Berlin: Springer-Verlag. p 125–136.
Hiller LP, Stover SM, Gibson VA, Gibeling JC, Prater CS, Hazelwood SJ, Yeh OC, Martin RB. 2003. Osteon pullout in the equine third metacarpal bone: Effects of ex vivo fatigue. J Orthop Res 21:481–488.
Hofmann A, Konrad L, Gotzen L, Printz H, Ramaswamy A, Hofmann C. 2003. Bioengineering human bone tissue using autogenous osteoblasts cultured on different biomatrices. J Biomed Mater Res 67:191–199.
Hogan HA. 1992. Micromechanics modeling of Haversian cortical bone properties. J Biomech 25:549–556.
Hosseini MM, Sodek J, Franke R-P, Davies JE. 2000. The structure and composition of the bone-implant interface. In: Davies JE, editor. Bone engineering. Toronto: Em Squared. p 295–304.
Holmes JL, Bachus KN, Bloebaum RD. 2000. Thermal effects of the electron beam and implications of surface damage in the analysis of bone tissue. Scanning 22:243–248.
Howell PG, Boyde A. 1994. Monte Carlo simulations of electron scattering in bone. Bone 15:285–291.
Howell PG, Boyde A. 1999. Surface roughness of preparations for back scattered-electron scanning electron microscopy: The image differences and their Monte Carlo simulation. Scanning 21:361–367.
Hunter GK, Goldberg HA. 1993. Nucleation of hydroxyapatite by bone sialoprotein. Proc Natl Acad Sci USA 90:8562–8565.
Hunter GK, Hauschka PV, Poole AR, Rosenberg LC, Goldberg HA. 1996. Nucleation and inhibition of hydroxyapatite by mineralized tissue proteins. Biochem J 317:59–64.
Ingram RT, Clarke BL, Fisher LW, Fitzpatrick LA. 1993. Distribution of noncollagenous proteins in the matrix of adult human bone: evidence of anatomic and functional heterogeneity. J Bone Miner Res 8:1019–1029.
Jaffe HL. 1972. Metabolic, degenerative, and inflammatory diseases of bones and joints. Philadelphia: Lea and Febiger. p 52–68.
Jee WSS. 1983. The skeletal tissues. In: Weiss L, editor. Histology: cell and tissue biology, 5th ed. New York: Elsevier Biomedical. p 200–255.
Jepsen KJ, Davy DT, Krzypow DJ. 1999. The role of the lamellar interface during torsional yielding of human cortical bone. J Biomech 32:303–310.
Jowsey J. 1960. Age changes in human bone. Clin Orthop 17:210–217.
Jowsey J. 1964. Variations in bone mineralization with age and disease. In: Frost HM, editor. Bone biodynamics. Boston: Little, Brown. p 461–479.
Jowsey J. 1966. Quantitative microradiography: a new approach in the evaluation of metabolic bone disease. Am J Med 40:485–491.
Kagayama M, Sasano Y, Akita H. 1993. Lectin binding in bone matrix of adult rats with special reference to cement lines. Tohoku J Exp Med 170:81–91.
Kanaya K, Okayama S. 1972. Penetration and energy-loss theory of electrons in solid targets. J Phys D Appl Phys 5:43–58.
Kato Y, Boskey A, Spevak L, Dallas M, Hori M, Bonewald LF. 2001. Establishment of an osteoid preosteocyte-like cell MLO-A5 that spontaneously mineralizes in culture. J Bone Miner Res 16:1622–1633.
Katz JL. 1980. Anisotropy of Young's modulus of bone. Nature 283: 106–107.
Katz JL. 1981. Composite material models for cortical bone. In: Cowin SC, editor. Mechanical properties of bone. New York: American Society of Mechanical Engineers. p 171–184.
Katz JL, Meunier A. 1993. Scanning acoustic microscope studies of the elastic properties of osteons and osteon lamellae. ASME Trans J Biomech Eng 115:543–548.
Kornblum SS, Kelly PJ. 1964. The lacunae and Haversian canals in tibial cortical bone from ischemic and non-ischemic limbs: a comparative microradiographic study. J Bone Joint Surg 46A:797–810.
Lacroix P. 1971. The internal remodeling of bones. In: Bourne GH, editor. The biochemistry and physiology of bone, vol. 3. New York: Academic Press. p 119–144.
Lakes RS, Katz JL. 1974. Interrelationships among the viscoelastic functions for anisotropic solids: application to calcified tissues and related systems. J Biomech 7:259–270.
Lakes RS, Katz JL. 1979. Viscoelastic properties of wet cortical bone: II, relaxation mechanisms. J Biomech 12:679–687.
Lakes RS, Saha S. 1979. Cement line motion in bone. Science 204: 501–503.
Lakes R. 1995. On the torsional properties of single osteons. J Biomech 28:1409–1410.
Lakes R. 2001. Viscoelastic properties of cortical bone. In: Cowin SC, editor. Bone mechanics handbook, 2nd ed. Boca Raton, FL: CRC Press. p 11.1–11.15.
Landis WJ, Glimcher MJ. 1978. Electron diffraction and electron probe microanalysis of the mineral phase of bone tissue prepared by anhydrous techniques. J Ultrastructural Res 63:188–233.
Les CM, Spence CA, Vance JL, Christopherson GT, Patel B, Turner AS, Divine GW, Fyhrie DP. 2004. Determinants of ovine compact bone viscoelastic properties: effects of architecture, mineralization, and remodeling. Bone 35:729–738.
Mabrey JD, Fitch RD. 1989. Plastic deformation in pediatric fractures: mechanism and treatment. J Pediatr Orthop 9:310–314.
Maj G, Toajari E. 1937. Osservazioni sperimentali sul meccanismo di resistenza del tessuto osseo lamellare compatto alle azioni meccaniche. Chir Org Mov 22:541–557.
Marotti G. 1996. The structure of bone tissues and the cellular control of their deposition. Ital J Anat Embryol 101:25–79.
Martin RB, Burr DB. 1982. A hypothetical mechanism for the stimulation of osteonal remodeling by fatigue damage. J Biomech 15: 137–139.
Martin RB, Burr DB. 1989. Structure, function, and adaptation of compact bone. New York: Raven Press.
Martin RB, Burr DB, Sharkey NA. 1998. Skeletal Tissue Mechanics. New York: Springer.
Martin RB. 1993. A finite element model for mineral transport into newly-formed bone. Trans 39th Orthop Res Soc 18:80.
Martin RB, Gibson VA, Stover SM, Gibeling JC, Griffin LV. 1996. Osteonal structure in the equine third metacarpus. Bone 19:165–171.
Mason MW, Skedros JG, Bloebaum RD. 1995. Evidence of strain-mode-related cortical adaptation in the diaphysis of the horse radius. Bone 17:229–237.
McKee MD, Nanci A. 1995. Osteopontin and the bone remodeling sequence: colloidal-gold immunocytochemistry of an interfacial extracellular matrix protein. Ann NY Acad Sci 760:177–189.
McKee MD, Nanci A. 1996a. Osteopontin at mineralized tissue interfaces in bone, teeth, and osseointegrated implants: ultrastructural distribution and implications for mineralized tissue formation, turnover, and repair. Microsc Res Tech 33:141–164.
McKee MD, Nanci A. 1996b. Osteopontin: an interfacial extracellular matrix protein in mineralized tissues. Connect Tissue Res 35:197–205.
Mellors RC. 1964. Electron probe microanalysis: 1, calcium and phosphorous in normal human cortical bone. Lab Invest 13:183–195.
Meunier PJ, Boivin G. 1997. Bone mineral density reflects bone mass but also the degree of mineralization of bone: therapeutic implications. Bone 21:373–377.
Meunier A, Katz JL, Christel P, Sedel L. 1998. A reflection scanning acoustic microscope for bone and bone-biomaterials interface studies. J Orthop Res 6:770–775.
Moyle DD, Bowden RW. 1984. Fracture of human femoral bone. J Biomech 17:203–213.
Muir P, Ruaux-Mason CP. 2000. Microcrack density and length in the proximal and distal metaphyses of the humerus and radius in dogs. Am J Vet Res 61:6–8.
Mulari MT, Qu Q, Harkonen PL, Vaananen HK. 2004. Osteoblast-like cells complete osteoclastic bone resorption and form new mineralized bone matrix in vitro. Calcif Tissue Int 75:253–261.
Mundy GR, Rodan SB, Majeska RJ, DeMartino S, Trimmier C, Martin TJ, Rodan GA. 1982. Unidirectional migration of osteosarcoma cells

with osteoblast characteristics in response to products of bone resorption. Calcif Tissue Int 34:542–546.
Murata K. 1974. Spatial distribution of backscattered electrons in the scanning electron microscope and electron microbe. J Appl Physiol 45:4110–4117.
Nanci A. 1999. Content and distribution of noncollagenous matrix proteins in bone and cementum: relationship to speed of formation and collagen packing density. J Struct Biol 126:256–259.
Nesbitt SA, Horton MA. 1997. Trafficking of matrix collagens through bone-resorbing osteoclasts. Science 276:266–269.
Nicholson WAP, Ashton BA, Hohling HJ, Quint P, Schreiber J. 1977. Electron microprobe investigations into the process of hard tissue formation. Cell Tissue Res 177:331–345.
Nicholson WAP, Dempster DW. 1980. Aspects of microprobe analysis of mineralized tissues. Scanning Electr Microsc Pt 2:517–533.
Nicolella DP, Nicholls AE, Lankford J, Davy DT. 2001. Machine vision photogrammetry: a technique for measurement of microstructural strain in cortical bone. J Biomech 34:135–139.
Norman TL, Vashishth D, Burr DB. 1995. Fracture toughness of human bone under tension. J Biomech 28:309–320.
Norman TL, Wang Z. 1997. Microdamage of human cortical bone: incidence and morphology in long bones. Bone 20:375–379.
Nyssen-Behets C, Arnould V, Dhem A. 1994. Hypermineralized lamellae below the bone surface: a quantitative microradiographic study. Bone 15:685–689.
O'Brien FJ, Taylor D, Lee TC. 2003. Microcrack accumulation at different intervals during fatigue testing of compact bone. J Biomech 36:973–980.
Ortner DJ, von Endt DW. 1971. Microscopic and electron microprobe characterization of the sclerotic lamellae in human osteons. Isr J Med Sci 7:480–482.
Pampena DA, Roberson KA, Litvinova O, Lajoie G, Goldberg HA. 2004. Inhibition of hydroxyapatite formation by osteopontin phosphopeptides. Biochem J 378:1083–1087.
Pankovich AM, Simmons DJ, Kulkarni VV. 1974. Zonal osteons in cortical bone. Clin Orthop 100:356–363.
Parfitt AM. 1983. The physiologic and clinical significance of bone histomorphometric data. In: Recker RR, editor. Bone histomorphometry: techniques and interpretation. Boca Raton, FL: CRC Press. p 143–223.
Parfitt AM. 1984. The cellular basis of bone remodeling: the quantum concept reexamined in light of recent advances in the cell biology of bone. Calcif Tissue Int 36:S37–S45.
Parfitt AM. 1994. Osteonal and hemi-osteonal remodeling: the spatial and temporal framework for signal traffic in adult human bone. J Cell Biochem 55:273–286.
Park HC, Lakes RS. 1986. Cosserat micromechanics of human bone: strain redistribution by a hydration sensitive constituent. J Biomech 19:385–397.
Payne CM, Cromey DW. 1990. Limitations of ZAF correction factors in the determination of calcium/phosphorus ratios: important forensic science considerations relevant to the analysis of bone fragments using scanning electron microscopy and energy-dispersive X-ray microanalysis. J Forens Sci 35:560–568.
Phelps JB, Hubbard GB, Wang X, Agrawal CM. 2000. Microstructural heterogeneity and the fracture toughness of bone. J Biomed Mater Res 51:735–741.
Philipson B. 1965. Composition of cement lines in bone. J Histochem Cytochem 13:270–281.
Piekarski K. 1970. Fracture of bone. J Appl Physiol 41:215–223.
Piekarski K. 1984. Fractography of bone. In: Hastings GW, Ducheyne P, editors. Natural living biomaterials. Boca Raton, FL: CRC Press. p 99–117.
Prendergast PJ, Huiskes R. 1996. Microdamage and osteocyte lacuna strain in bone: a microstructural finite element analysis. ASME Trans J Biomech Eng 118:240–246.
Pritchard JJ. 1972. General histology of bone. In: Bourne GH, editor. The biochemistry and physiology of bone, 2nd ed., vol. 1. New York: Academic Press. p 1–20.
Reid SA, Boyde A. 1987. Changes in the mineral density distribution in human bone with age: image analysis using backscattered electrons in the SEM. J Bone Miner Res 2:13–22.
Rho JY, Zioupos P, Currey JD, Pharr GM. 1999. Variations in the individual thick lamellar properties within osteons by nanoindentation. Bone 25:295–300.
Rosenberg AE. 1994. Skeletal system and soft tissue tumors. In: Cotran RS, Kumar V, Robbins SL, Schoen FJ, editors. Robbins pathologic basis of disease, 5th ed. Philadelphia: W.B. Saunders. p 1213–1271.
Roschger P, Eschberger J, Plenk H Jr. 1993. Formation of ultracracks in methacrylate-embedded undecalcified bone samples by exposure to aqueous solutions. Cells Mater 3:361–365.
Roschger P, Plenk H Jr, Klaushofer K, Eschberger J. 1995. A new scanning electron microscopy approach to the quantification of bone mineral distribution: backscattered electron image grey-levels correlated to calcium Kα-line intensities. Scanning Microsc 9:75–88.
Roschger P, Fratzl P, Klaushofer K, Rodan G. 1997. Mineralization of cancellous bone after alendronate and sodium fluoride treatment: a quantitative backscattered electron imaging study on minipig ribs. Bone 20:393–397.
Ruff CB, Hayes WC. 1983. Cross-sectional geometry of Pecos Pueblo femora and tibiae: a biomechanical investigation—method and general patterns of variation. Am J Phys Anthropol 60:359–381.
Saha S. 1977. Longitudinal shear properties of human compact bone and its constituents and the associated failure mechanisms. J Mater Sci 12:1798–1806.
Salo J, Lehenkari P, Mulari M, Metsikko K, Vaananen HK. 1997. Removal of osteoclast bone resorption products by transcytosis. Science 276:270–273.
Schaffler MB, Burr DB, Frederickson RG. 1987. Morphology of the osteonal cement line in human bone. Anat Rec 217:223–228.
Schaffler MB, Choi K, Milgrom C. 1995. Aging and matrix microdamage accumulation in human compact bone. Bone 17:521–525.
Schmidt WJ. 1959. Grenzscheiden der lakunen und kittlinien des knochengewebes: polarisationsoptische analyse kollagenfreier kongorrotgefarbter schliffe. Z Zellforsch 50:275–296.
Simmons DJ. 1985. Options for bone aging with the microscope. Yearbook Phys Anthropol 28:249–263.
Simmons ED Jr, Pritzker KPH, Grynpas MD. 1991. Age-related changes in the human femoral cortex. J Orthop Res 9:155–167.
Sissons HA, Jowsey J, Stewart L. 1960. The microradiographic appearance of normal bone at various ages. In: Engström A, Coslett V, Pattee H, editors. X-ray microscopy and X-ray microanalysis: proceedings of the Second International Symposium. New York: Elsevier. p 206–215.
Sissons HA. 1962. Age changes in the structure and mineralization of bone tissue in man. In: McLean FC, LaCroix P, Budy AM, editors. Radioisotopes and bone. London: Blackwell Scientific Publications. p 443–465.
Sit S, Bizios R, Vashishth D. 2003. Is bone resorption in human cortical bone limited by cement lines? Trans 49th Orthop Res Soc 28:384.
Skedros JG, Bloebaum RD, Bachus KN, Boyce TM. 1993a. The meaning of gray levels in backscattered electron images of bone. J Biomed Mater Res 27:47–56.
Skedros JG, Bloebaum RD, Bachus KN, Boyce TM, Constantz B. 1993b. Influence of mineral content and composition on gray levels in backscattered electron images of bone. J Biomed Mater Res 27:57–64.
Skedros JG, Mason MW, Bloebaum RD. 1994. Differences in osteonal micromorphologies between tensile and compressive cortices of a bending skeletal system: indications of potential strain-specific differences in bone microstructure. Anat Rec 239:47–63.
Skedros JG, Durand P, Bloebaum RD. 1995. Hypermineralized peripheral lamellae in primary osteons of deer antler: potential functional analogues of cement lines in mammalian secondary bone. J Bone Miner Res 10(Suppl 1):S441.
Skedros JG, Mason MW, Nelson MC, Bloebaum RD. 1996. Evidence of structural and material adaptation to specific strain features in cortical bone. Anat Rec 246:47–63.
Skedros JG, Hunt KJ, Bloebaum RD. 2004. Relationships of loading history and structural and material characteristics of bone: development of the mule deer calcaneus. J Morphol 259:281–307.
Smith JW. 1963. Age changes in the organic fraction of bone. J Bone Joint Surg 45B:761–769.

Sobelman OS, Gibeling JC, Stover SM, Hazelwood SJ, Yeh OC, Shelton DR, Martin RB. 2004. Do microcracks decrease or increase fatigue resistance in cortical bone? J Biomech 27:1295–1303.
Sokoloff L. 1973. A note on the histology of cement lines. In: Kenedi RM, editor. Perspectives in biomedical engineering. Baltimore, MD: University Park Press. p 135–138.
Stout S, Simmons DJ. 1979. Use of histology in ancient bone research. Yearbook Phys Anthropol 22:228–249.
Sumner DR, Bryan JM, Urban RM, Kuszak JR. 1990. Measuring the volume fraction of bone ingrowth: a comparison of three techniques. J Orthop Res 8:448–452.
Terai K, Takano-Yamamoto T, Ohba Y, Hiura K, Sugimoto M, Sato M, Kawahata H, Inaguma N, Kitamura Y, Nomura S. 1999. Role of osteopontin in bone remodeling caused by mechanical stress. J Bone Miner Res 14:839–849.
Tran Van P, Vignery A, Baron R. 1982. An electron microscopic study of the bone remodeling sequence in the rat. Cell Tissue Res 225: 283–292.
Trotter M, Hixon BB. 1974. Sequential changes in weight, density, and percentage ash weight of human skeletons from an early fetal period through old age. Anat Rec 179:1–18.
Tye CE, Rattray KR, Warner KJ, Gordon JAR, Sodek J, Hunter GK, Goldberg HA. 2003. Delineation of the hydroxyapatite-nucleating domains of bone sialoprotein. J Biol Chem 278:7949–7955.
Vajda EG, Skedros JG, Bloebaum RD. 1995. Consistency in calibrated backscattered electron images of calcified tissues and minerals analyzed in multiple imaging sessions. Scanning Microsc 9:741–755.
Vajda EG, Bloebaum RD, Skedros JG. 1996. Validation of energy dispersive X-ray spectrometry as a method to standardize backscattered electron images of bone. Cells Mater 6:79–92.
Vajda EG, Bloebaum RD, Skedros JG. 1998. Errors in backscattered electron analysis of bone standardized by energy-dispersive X-ray spectrometry. Scanning 20:527–535.
Vajda EG, Humphrey S, Skedros JG, Bloebaum RD. 1999. Influence of topography and specimen preparation on backscattered electron images of bone. Scanning 21:379–386.
Von Ebner V. 1875 Uber den feineren bau der knochensubstanz. Sitzungsberichte Deutsch Akad Wissenschaften Berlin 72:49–138.
Villanueva AR, Sypitkowski C, Parfitt AM. 1986. A new method for identification of cement lines in undecalcified, plastic embedded sections of bone. Stain Technol 61:83–88.
Vose GP, Baylink DJ. 1970. Effect of fibrillar structure of pericanalicular and intercanalicular bone on X-ray absorption. Anat Rec 166:239–246.
Wang Z, Norman TL. 1996. In vivo microdamage of human cortical bone supports the hypothesis that cement lines "trap" cracks. Trans 42nd Orthop Res Soc 21:594.
Weidenreich F. 1930. Das knochengewebe. In: von Mollendorff W, editor. Mollendorff Handbuch der mikroskopischen Anatomie des Menschen, vol. 2, pt. 2. Berlin: Verlag Julius Springer. p 391–520.
Weinmann JP, Sicher H. 1955. Bone tissue. In: Bone and bones. fundamentals of bone biology, 2nd ed. St. Louis, MO: C.V. Mosby. p 18–46.
Wong FL, Elliott JC. 1997. Theoretical explanation of the relationship between backscattered electron and X-ray linear attenuation coefficients in calcified tissues. Scanning 19:541–546.
Xiao Y, Haase H, Young WG, Bartold PM. 2004. Development and transplantation of a mineralized matrix formed by osteoblasts in vitro for bone regeneration. Cell Transplant 12:15–25.
Yeager JA. 1971. Bone morphology and mineral homeostasis, In: Moyers RE, Krogman WM, editors. Cranio-facial growth in man: part II, the biology of bone. New York: Pergamon Press. p 27–32.
Yeni YN, Brown CU, Wang Z, Norman TL. 1997. The influence of bone morphology on fracture toughness of the human femur and tibia. Bone 21:453–459.
Yeni YN, Norman TL. 2000. Calculation of porosity and osteon cement line effects on the effective fracture toughness of cortical bone in longitudinal crack growth. J Biomed Mat Res 51:504–509.
Zagba-Mongalima G, Goret-Nicaise M, Dhem A. 1988. Age change in human bone: a microradiographic and histological study of subperiosteal and periosteal calcifications. Gerontology 34:264–276.
Zhou H, Chernecky R, Davies JE. 1994. Deposition of cement at reversal lines in rat femoral bone. J Bone Miner Res 9:367–374.
Zhu X-L, Ganss B, Goldberg HA, Sodek J. 2001. Synthesis and processing of bone sialoproteins during de novo bone formation in vitro. Biochem Cell Biol 79:737–746.
Zioupos P, Currey JD. 1994. The extent of microcracking and the morphology of microcracks in damaged bone. J Mater Sci 29:978–986.

APPENDIX: CEMENT LINE TERMINOLOGY
Cement (Reversal) Lines, Resting Lines, Arrest Lines, Hypermineralized Lines

Most bone histologists distinguish cement lines of secondary bone from other similarly appearing distinct morphologic lines or seams. For example, resting (or arrest) lines, although they appear relatively highly mineralized and are present in secondary bone, typically do not exhibit crenulations and are relatively thicker than the traditional crenulated cement lines of secondary bone (Weinmann and Sicher, 1955; Lacroix, 1971; Zagba-Mongalima et al., 1988; McKee and Nanci, 1995). Furthermore, resting lines are considered to be either the result of a reduction in the rate of bone formation or cessation of bone formation (arrest lines) not proceeded by a resorptive event (Frost, 1963, 1973; Kornblum and Kelly, 1964; Jaffe, 1972; Pankovich et al., 1974; Parfitt, 1983; de Ricqlès et al., 1991; Nyssen-Behets et al., 1994; McKee and Nanci, 1995). However, the terms "cement line" (reversal line) and "resting/arrest line" have been used synonymously in recent literature (Zhou et al., 1994; McKee and Nanci, 1995). Additionally, there are investigators who have considered cement lines as the material that is deposited at initial sites of bone formation, whether the forming bone is secondary or primary (Frasca et al., 1981a; McKee and Nanci, 1995; Davies, 1996).

Cement lines at reversal sites are produced by differentiating osteogenic cells. Resting/arrest lines are secreted by already differentiated osteoblasts. Consequently, the relative synthetic capacity of these cell types may differ (Marotti, 1996; Hosseini et al., 2000; Kato et al., 2001; Hofmann et al., 2003). For example, the relative differentiation of these osteogenic cells has been used to explain why resting lines contain more bone sialoprotein than reversal lines (Hosseini et al., 2000). Hosseini et al. (2000: p. 301) also noted: "That cement lines are devoid of collagen has long been recognized (Weidenreich, 1930). It is not surprising, therefore, that cells derived from undifferentiated perivascular mesenchyme, and which are not yet expressing the full osteogenic phenotype, do not assemble a collagenous extracellular matrix."

Classically defined cement lines can also be distinguished from other apparently hypermineralized lines. Although having a similar microradiographic appearance to cement and resting lines, hypermineralized seams of tissue located short distances from central canals of completely formed secondary osteons have been called hypermineralized lamellae (Dhem, 1980; Dhem and Robert, 1986; Nyssen-Behets et al., 1994). Unlike cement lines and resting lines, hypermineralized lamellae in human bone can be traversed by osteocyte lacunae and can be associated with hypermineralization around osteocyte lacunae (Jowsey, 1964; Dhem and Robert, 1986; Nyssen-Behets et al., 1994). The term "hypermineralized lamellae" has also been used to describe the prevalent highly mineralized seams observed within primary bone of mature deer antler (Skedros et al., 1995).